INTERNATIONAL JOURNAL FOR NUMERICAL METHODS IN ENGINEERING
Int. J. Numer. Meth. Engng 2002; **55**:1129–1166 (DOI: 10.1002/nme.534)

Implicit J_2-bounding surface plasticity using Prager's translation rule

Francisco J. Montáns[1,*,†] and Ronaldo I. Borja[2]

[1]*Escuela Técnica Superior de Ingenieros Industriales, Universidad de Castilla La Mancha, Edificio Politécnica, Campus Universitario, 13071 Ciudad Real, Spain*
[2]*Department of Civil and Environmental Engineering, Stanford University, Stanford, CA 94305-4020, U.S.A.*

SUMMARY

A bounding surface J_2-plasticity model that uses Prager's translation rule is presented. The model preserves Masing's rules and is developed from the same ideas as classical infinitesimal J_2-plasticity, resulting in the same formulation with the exception of the algorithm for the computation of the hardening function. Instead of utilizing a loading surface as in a previous formulation, hardening surfaces are introduced; the formulation is similar to that of multilayer plasticity using Prager's rule, presented in previous work. An implicit algorithm based on the radial return concept is used, and the consistent elastoplastic tangent is also developed in closed form. Examples illustrating anisotropic behaviour are presented and compared to that predicted by a multilayer J_2-plasticity model. The model is also applied to a soil dynamics problem to show the robustness of the algorithm and its applicability to complex loading. Copyright © 2002 John Wiley & Sons, Ltd.

KEY WORDS: computational plasticity; implicit integration; bounding surface plasticity; multiaxial behaviour; finite elements

1. INTRODUCTION

One of the most compelling and challenging problems in computational plasticity is the development of efficient, robust, and mathematically well-founded anisotropic plasticity models capable of extending the uniaxial behaviour of materials to multiaxial cyclic loading conditions. The classical bilinear kinematically hardening-type J_2-plasticity model is the simplest of such. Associative J_2-plasticity is motivated by the principle of maximum plastic dissipation and the existence of potential energy functions [1]. Possibly because of this, the currently well-known implicit return mapping schemes allow for efficient implementation of the bilinear model. Unfortunately, a bilinear model is not acceptable for some materials, specially under multiaxial cyclic loading [2]. This is especially true in soils [3, 4]. To describe the non-linearity of the stress–strain curve, non-linear hardening functions are often employed;

*Correspondence to: Francisco J. Montáns, Escuela Técnica Superior de Ingenieros Industriales, Universidad de Castilla La Mancha, Edificio Politécnica, Campus Universitario, 13071 Ciudad Real, Spain
†E-mail: francisco.montans@uclm.es

Received 4 June 2001
Revised 29 November 2001
Accepted 19 December 2001

however, they are generally unacceptable since Masing's rules [3] are not properly preserved. Thus, researchers and engineers frequently choose other models. Two formulations of those seem to have found success in general-purpose finite element codes: multilayer (or overlay) plasticity and bounding surface plasticity.

The multilayer plasticity model was developed by Mróz [5] and Iwan [6] and assumes the existence of several yield surfaces (or loading surfaces), each of which has an associated hardening modulus. Apart from making use of new concepts such as the loading surface, multilayer plasticity also requires an *ad hoc* translation rule, which makes an implicit numerical integration difficult to implement [7]. Quite recently, an implicit *ad hoc* reformulation of the translation rule has allowed for a fully implicit numerical implementation of the multilayer plasticity theory [8, 9]. Unfortunately, the rule implied a maximum admissible ratio of two between the radii of two adjacent surfaces. Just recently [8], multilayer plasticity has been reformulated in the context of classical J_2-plasticity, motivated from the same concepts. It does not make use of the concept of loading surface (the yield surface acts always as such) and utilizes Prager's rule for translation. This has permitted the reduction of multilayer plasticity to classical J_2-plasticity, except for the computation of the hardening function. The development of a fully implicit algorithm does not impose any requirement in the size of the surfaces (that now act just as hardening surfaces) and has a consistently linearized tangent to preserve the convergence of second order of the Newton algorithms.

Bounding surface plasticity was developed by Dafalias and Popov [10] and independently by Krieg [11], and is arguably simpler and easier to implement than multisurface plasticity models. The use of only two surfaces and an interpolation parameter allows for smooth characterization of stress–strain relationships. Furthermore, bounding surface models do not necessitate a large number of surfaces to represent the stress–strain curve with acceptable accuracy. Unfortunately, similar difficulties have been encountered with these models, particularly with implicit numerical implementation, although this has been addressed in the literature [12–16]. Nonetheless, they still make use of the concept of loading surface or an equivalent idea, and have three intrinsic behavioural problems: overshooting phenomena, lack of the preservation of Masing's rules and inconsistent out-of-phase behaviour [2, 17, 18]. The overshooting phenomena has been eliminated through the use of virtual positioning of the bounding surface [17], but the need for a 'loading surface' has not fully been eliminated.

A comparison of the multilayer models using Mróz's translation rule and Prager's rule also revealed different behavioural patterns in the non-proportional case (see Reference [8]). Prager's translation rule results in a behaviour that relates stress increments to strain increments more closely, mainly when the size of the yield surface is small. This is a frequently desired feature in soils [14], and it has been sometimes termed as hypoplasticity in the context of bounding surface plasticity [19, 20].

In this work a bounding surface model similar to the multilayer model of Reference [8] is presented. The model uses a virtual bounding surface to preserve the Masing behaviour (as in a multilayer model). It is associative both in hardening and flow rules, motivated by the principle of maximum plastic dissipation. As in the multilayer model, the equations are the same as those of classical J_2-plasticity, except for the hardening function which is computed from the interpolation parameter and the internal variables. The computation of the hardening tensor in the model is conceptually identical to the one in multilayer plasticity, excluding the obvious differences between both models. In fact it assumes the existence of an infinite

number of hardening surfaces, each one with its associated hardening modulus. The present model uses Prager's translation rule for the yield surface. The consistency equation and the unloading condition are enforced only on the yield surface, and the hardening surfaces are used to determine the hardening modulus and not the loading–unloading condition. The contact point for the surfaces and the stress tensor are not necessarily the same. Both models may be viewed as a way of computing the hardening function of classical J_2-plasticity.

A fully implicit integration algorithm based on the radial return scheme is also presented. The algorithm results in a consistent elastoplastic tangent operator that allows a quadratic convergence to be captured in the global Newton-type algorithm. Unfortunately, the generality of the possible hardening functions and the integrations to be performed require a numerical integration scheme that needs to be included in the overall algorithm, since it affects both the stress-point-level tangent (to obtain the consistency parameter) and the global one. The chosen integration rule is a composite Simpson rule.

Numerical examples are presented that aim to demonstrate both the behavioural features and the robustness of the model. In the stress-point-level examples, in which the material routine is executed alone and the stress-path is prescribed, the model is compared to multilayer plasticity using both Mróz's and Prager's rules. To demonstrate the robustness of the algorithm, soil dynamics is used because it is a severe test; the non-linearity of the stress–strain curve is strong, the size of the yield surface is virtually vanishing, and the path is strongly non-proportional and irregular. To allow for a comparison with other models [8, 21] and to run a case-study problem, the Lotung LSST07 seismic event has been analysed.

2. MODEL DEVELOPMENT

Since the model is developed from the notion of bounding surface plasticity, the general features of the latter type of models are first briefly reviewed.

2.1. Bounding surface J_2-plasticity

The bounding surface concept relies on the existence of a domain in which the stresses are constrained. The existence of this domain forces the hardening modulus to have a zero value (or a minimum value) once the stress tensor reaches the surface, whereas when the stresses are on the yield surface the hardening modulus attains its maximum value. When the stresses are in the domain between both surfaces, the hardening function is interpolated using a function that depends on a parameter that somehow measures the distance of the tensor to the surfaces.

In the present model, both the bounding surface and the yield surface are assumed to be circles on the π-plane. The back-stresses of the surfaces are denoted by $\boldsymbol{\beta}$ and $\boldsymbol{\alpha}$, respectively, whereas the norm-like radii are denoted by R and r, respectively. Thus, the yield surface is given by

$$f(\boldsymbol{\sigma}) := \|\boldsymbol{\sigma} - \boldsymbol{\alpha}\| - r = 0 \tag{1}$$

where $\boldsymbol{\sigma}$ is the deviatoric stress tensor, given by

$$\boldsymbol{\sigma} = \boldsymbol{\sigma}^{\mathrm{f}} - \tfrac{1}{3}\,\mathrm{tr}(\boldsymbol{\sigma}^{\mathrm{f}})\mathbf{I} \tag{2}$$

where $\boldsymbol{\sigma}^{\mathrm{f}}$ is the complete ('full') stress tensor which includes the volumetric part. Similarly, the bounding surface is

$$f_{\mathrm{b}}(\hat{\boldsymbol{\sigma}}) := \|\hat{\boldsymbol{\sigma}} - \boldsymbol{\beta}\| - R = 0 \tag{3}$$

where $\hat{\boldsymbol{\sigma}}$ is usually called image stress tensor.

A homology is established in the stress domain between both surfaces and the centre of the homology, $\boldsymbol{\sigma}_0$, usually termed unloading stress tensor. The tensors $\hat{\boldsymbol{\sigma}}$, $\boldsymbol{\sigma}$ and $\boldsymbol{\sigma}_0$ are co-linear in the sense that

$$\hat{\boldsymbol{\sigma}} = \boldsymbol{\sigma} + \kappa(\boldsymbol{\sigma} - \boldsymbol{\sigma}_0) \tag{4}$$

Thus, the scalar parameter κ may be obtained from $\boldsymbol{\sigma}$ and $\boldsymbol{\sigma}_0$ as

$$\kappa = \frac{\|\hat{\boldsymbol{\sigma}} - \boldsymbol{\sigma}\|}{\|\boldsymbol{\sigma} - \boldsymbol{\sigma}_0\|} \tag{5}$$

where $\hat{\boldsymbol{\sigma}}$ is obtained from Equation (4). The hardening function, denoted by the symbol $H(\kappa)$, may be written in terms of κ, interpolating the values between those associated to the yield surface and those on the bounding surface [14] (see Figure 1). Consequently, the surfaces for which the hardening function is constant are circles homological with the previous ones (see References [14, 17]). Alternatively, κ may be re-written in terms of a more tangible parameter p, the normalized-to-R radius of the surface for which the hardening function is constant (hardening surface) and shown to be [17]

$$p = \frac{1}{1 + \kappa} \tag{6}$$

The centre of the hardening surface is given by

$$\boldsymbol{\alpha}_p = \boldsymbol{\sigma}_0 + p(\boldsymbol{\beta} - \boldsymbol{\sigma}_0) \tag{7}$$

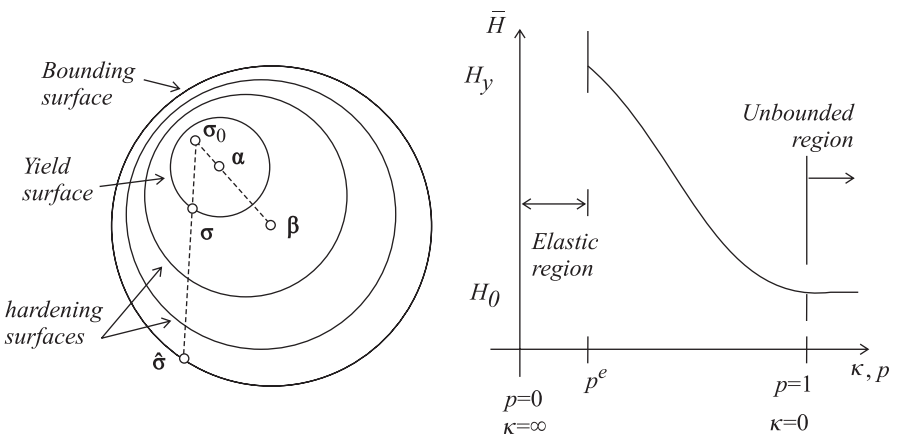

Figure 1. Geometric set-up of a bounding surface plasticity model and typical hardening function depending on the homology parameter.

and its radius by pR. Traditionally, the hardening surfaces

$$f_p(\boldsymbol{\sigma}) := \|\boldsymbol{\sigma} - \boldsymbol{\alpha}_p\| - pR = 0 \tag{8}$$

have been considered as loading surfaces, i.e. when $\dot{\boldsymbol{\sigma}} : \partial f_p / \partial \boldsymbol{\sigma} < 0$ then an unloading process takes place and a new homology is generated. Nonetheless, the potential surface which gives the direction of the plastic strains increment has been considered as the hardening surface or the yield surface (which in some cases may be vanishing, see Reference [14]).

2.2. Virtual bounding surface

After a process of loading through the virgin loading curve, when an unloading process takes place in a classical bounding surface model the homological ratio between the new unloading curve and the virgin stress-strain curve is given by (see Reference [17])

$$\eta = \frac{R + \hat{\mathbf{n}} : (\boldsymbol{\beta} - \boldsymbol{\sigma}_0)}{R} \tag{9}$$

where $\hat{\mathbf{n}}$ is the tensor normal to the yield surface. In uniaxial loading the previous expression yields

$$\eta = \frac{R \pm \|\boldsymbol{\beta} - \boldsymbol{\sigma}_0\|}{R} \tag{10}$$

and this ratio equals the value 2 only if unloading takes place at the bounding surface. Otherwise, the adopted value is given somewhat arbitrarily by the geometric setup of the model. The value of 2 is a reference value because it is the one that produces stable and closed loops and, thus, it is one of Masing's rules [3]. Constant values bigger than 2 yield cyclic hardening and values smaller than 2 yield cyclic softening, see Figure 2. Different arbitrary values induce the typical overshooting (or 'under'-shooting) phenomena in classical bounding surface models. Thus, as a point of departure, a desired η value is 2 for every stress level. Note that cyclic hardening/softening may be obtained through a hardening/softening for the radius of the bounding surface R.

To obtain the desired value of $\eta = 2$ for uniaxial loading, it is necessary that $\|\boldsymbol{\beta} - \boldsymbol{\sigma}_0\| = R$. Since the unloading (reference) stress $\boldsymbol{\sigma}_0$ cannot be modified, the virtual bounding surface model adopts a modified (virtual) value for $\boldsymbol{\beta}$. For example, in uniaxial loading, when unloading is detected $\boldsymbol{\beta} = \boldsymbol{\sigma}_0 - R\hat{\mathbf{n}}$. This value is transitory, unreal, and serves as a tool to use the same description for the hardening function. Once the previous level of stresses is again reached, the old $\boldsymbol{\beta}$ value is recovered and, therefore, the original $\eta = 1$ of the virgin curve is restored. Note that with this strategy, the overshooting phenomena inherent to bounding surface plasticity is overcome.

2.3. Geometric layout

The model is developed based on the assumption that there exist an infinite number of surfaces, each one with radius pR, with an associated hardening modulus $H_p(p)$ and that translate once they are reached by the yield function. The infinite number of hardening surfaces (one for each p value) inside the 'active' one translate in the direction given by $\hat{\mathbf{m}}$ (see Figure 3), defined by the contact point between the yield surface (which translates using Prager's rule) and the last (outer) hardened surface [8]. This contact point is not necessarily the one representing

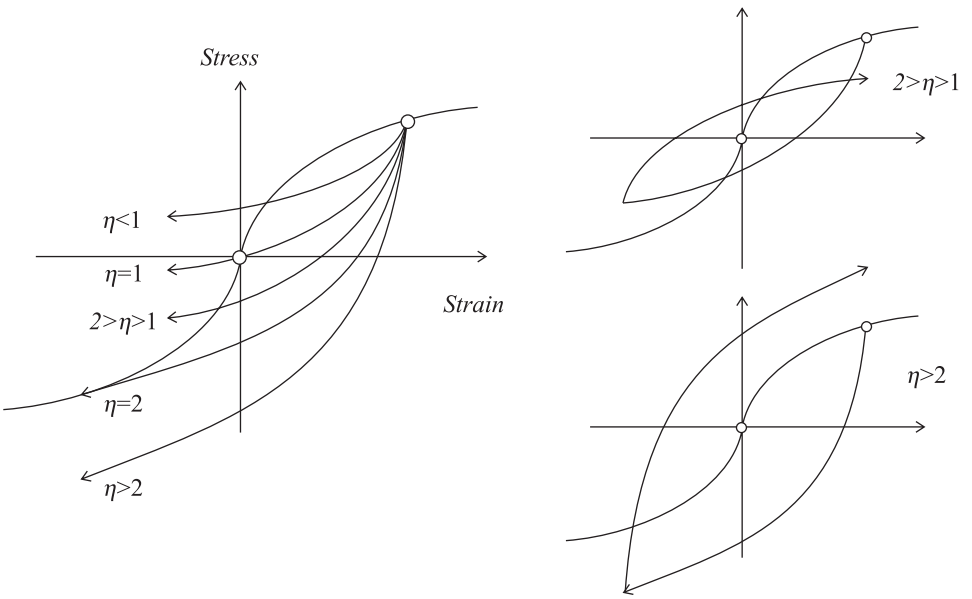

Figure 2. Influence of the new homology ratio η in the uniaxial stress–strain curve.

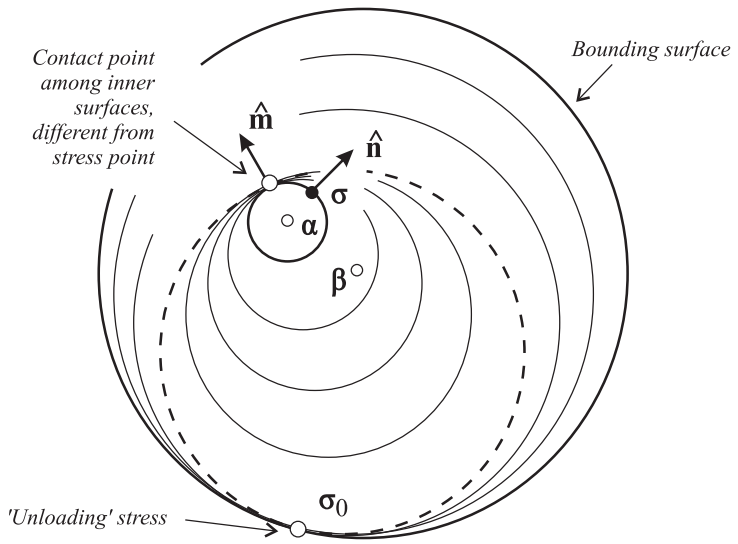

Figure 3. Position of the hardening surfaces, contact direction $\hat{\mathbf{m}}$ and flow direction $\hat{\mathbf{n}}$. Dotted circle is the 'active' hardening surface.

the stress tensor. The unloading stress tensor $\boldsymbol{\sigma}_0$ and the back stress of the bounding surface $\boldsymbol{\beta}$ define the initial position of the surfaces just after an 'unloading' event. These positions are defined consistently to preserve the position of the yield surface (as the hardening surface with radius $p^{\mathrm{e}}R$) and the desired $\eta = 2$.

3. CONTINUUM FORMULATION

We assume the classical additive decomposition of the small strain tensor rate $\dot{\boldsymbol{\varepsilon}}$ into an elastic part $\dot{\boldsymbol{\varepsilon}}^{\mathrm{e}}$ and a plastic part $\dot{\boldsymbol{\varepsilon}}^{\mathrm{p}}$:

$$\dot{\boldsymbol{\varepsilon}} = \dot{\boldsymbol{\varepsilon}}^{\mathrm{e}} + \dot{\boldsymbol{\varepsilon}}^{\mathrm{p}} \tag{11}$$

The dissipation function is defined, in the context of small strain plasticity as

$$\dot{\mathscr{D}}^{\mathrm{p}} = \boldsymbol{\sigma} : \dot{\boldsymbol{\varepsilon}}^{\mathrm{p}} + \boldsymbol{\alpha} : \dot{\boldsymbol{\xi}} \tag{12}$$

where $\dot{\boldsymbol{\xi}}$ is the strain-like internal variables tensor, work-conjugate of the internal variables tensor $\boldsymbol{\alpha}$ (the back-stress tensor). The principle of maximum dissipation implies (see for example Reference [1]), apart from the convexity of the yield function, associative flow rule

$$\dot{\boldsymbol{\varepsilon}}^{\mathrm{p}} = \dot{\gamma}\,\frac{\partial f}{\partial \boldsymbol{\sigma}} =: \dot{\gamma}\hat{\mathbf{n}}, \quad \text{where } \boldsymbol{\sigma} = \mathbb{C} : \boldsymbol{\varepsilon}^{\mathrm{e}} \tag{13}$$

associative hardening in the sense that

$$\dot{\boldsymbol{\xi}} = \dot{\gamma}\,\frac{\partial f}{\partial \boldsymbol{\alpha}} = -\dot{\gamma}\hat{\mathbf{n}}, \quad \text{where } \dot{\boldsymbol{\alpha}} = -\mathbb{H} : \dot{\boldsymbol{\xi}} \tag{14}$$

and the Kuhn–Tucker loading/unloading conditions,

$$\dot{\gamma} \geqslant 0, \quad f(\boldsymbol{\sigma}, \boldsymbol{\alpha}) \leqslant 0, \quad \dot{\gamma} f(\boldsymbol{\sigma}, \boldsymbol{\alpha}) = 0 \tag{15}$$

where $\mathbb{C}$ and $\mathbb{H}$ are, respectively, the fourth-order elastic tensor and the fourth-order hardening tensor, defined from the complementary stored energy function ψ_{ε} and complementary hardening potential ψ_{ξ} as

$$\mathbb{C}^{-1} := \frac{\partial^2 \psi_{\varepsilon}}{\partial \boldsymbol{\sigma}\,\partial \boldsymbol{\sigma}}, \quad \mathbb{H}^{-1} := \frac{\partial^2 \psi_{\xi}}{\partial \boldsymbol{\alpha}\,\partial \boldsymbol{\alpha}} \tag{16}$$

It is assumed that both tensors are positive-definite and $\mathbb{C}$ is constant in the range of interest.

As in classical 3D/plane strain kinematically hardened J_2-plasticity, it is assumed that the yield surface translates in the stress space using Prager's rule:

$$\dot{\boldsymbol{\alpha}} = \dot{\lambda}\hat{\mathbf{n}} \tag{17}$$

where $\dot{\lambda}$ is a parameter to be determined. From Equation (14)

$$\dot{\boldsymbol{\alpha}} = \dot{\lambda}\hat{\mathbf{n}} = \dot{\gamma}\mathbb{H} : \hat{\mathbf{n}} \tag{18}$$

that means that $\mathbb{H}$ must have at least one eigenvalue in $\hat{\mathbf{n}}$ which will be denoted by H. Aside, in unloading or neutral loading directions the elastic behaviour is recovered again, this means that for any $\hat{\mathbf{r}}$ such that $\hat{\mathbf{r}} : \hat{\mathbf{n}} \leqslant 0$, $\hat{\mathbf{r}} : \mathbb{H}^{-1} : \hat{\mathbf{r}} = 0$. Denoting by $\langle \hat{\mathbf{n}} \otimes \hat{\mathbf{n}} \rangle$ the fourth-order tensor such that $\langle \hat{\mathbf{n}} \otimes \hat{\mathbf{n}} \rangle : \hat{\mathbf{r}} = \hat{\mathbf{r}} : \langle \hat{\mathbf{n}} \otimes \hat{\mathbf{n}} \rangle = \langle \hat{\mathbf{n}} : \hat{\mathbf{r}} \rangle \hat{\mathbf{n}}$ and that $\hat{\mathbf{r}} : \langle \hat{\mathbf{n}} \otimes \hat{\mathbf{n}} \rangle : \hat{\mathbf{r}} = (\langle \hat{\mathbf{r}} : \hat{\mathbf{n}} \rangle)^2$, a hardening tensor of the form

$$\mathbb{H} = H \langle \hat{\mathbf{n}} \otimes \hat{\mathbf{n}} \rangle \quad \text{with } H > 0 \tag{19}$$

fulfils the requirements (note that H includes the typical $\frac{2}{3}$ factor of the uniaxial comparison). In consequence, $\dot{\lambda} = \dot{\gamma} H$.

The consistency equation is

$$\dot{f} = \hat{\mathbf{n}} : (\dot{\boldsymbol{\sigma}} - \dot{\boldsymbol{\alpha}}) \tag{20a}$$

$$= \hat{\mathbf{n}} : \mathbb{C} : (\dot{\boldsymbol{\varepsilon}} - \dot{\boldsymbol{\varepsilon}}^{\mathrm{p}}) - \dot{\gamma}\hat{\mathbf{n}} : \mathbb{H} : \hat{\mathbf{n}} \tag{20b}$$

$$= \hat{\mathbf{n}} : \mathbb{C} : \dot{\boldsymbol{\varepsilon}} - \dot{\gamma}\hat{\mathbf{n}} : \mathbb{C} : \hat{\mathbf{n}} - \dot{\gamma}\hat{\mathbf{n}} : \mathbb{H} : \hat{\mathbf{n}} \geqslant 0 \tag{20c}$$

Therefore, the consistency parameter may be factored-out as

$$\dot{\gamma} = \frac{\langle \hat{\mathbf{n}} : \mathbb{C} : \dot{\boldsymbol{\varepsilon}} \rangle}{\hat{\mathbf{n}} : \mathbb{C} : \hat{\mathbf{n}} + \hat{\mathbf{n}} : \mathbb{H} : \hat{\mathbf{n}}} = \frac{2\mu}{2\mu + H} \langle \hat{\mathbf{n}} : \dot{\boldsymbol{\varepsilon}} \rangle \geqslant 0 \tag{21}$$

where μ is the shear modulus and $\langle \cdot \rangle$ is the Macauley bracket function such that for x real number, $\langle x \rangle := \frac{1}{2}(x + |x|)$. This expression is coincident with the one of J_2-plasticity. The elastoplastic tangent moduli tensor is

$$\mathbb{C}^{\mathrm{ep}} = \mathbb{C} - \frac{\mathbb{C} : \hat{\mathbf{n}} \otimes \mathbb{C} : \hat{\mathbf{n}}}{\hat{\mathbf{n}} : \mathbb{C} : \hat{\mathbf{n}} + \hat{\mathbf{n}} : \mathbb{H} : \hat{\mathbf{n}}} \tag{22}$$

as in associative (both in flow and hardening rules) plasticity.

In this model, as in Reference [8], we assume an additive decomposition in the strain-like internal variables ($\dot{\boldsymbol{\xi}} = -\dot{\boldsymbol{\varepsilon}}^{\mathrm{p}}$ as it can be easily seen) such that

$$\dot{\boldsymbol{\xi}} = \dot{\boldsymbol{\xi}}_y + \dot{\boldsymbol{\xi}}_b \tag{23}$$

Since the model is associative, Equation (14a) must be preserved, so we can write

$$\dot{\boldsymbol{\xi}}_y = -\dot{\gamma}_y \hat{\mathbf{n}}, \quad \dot{\boldsymbol{\xi}}_p = -\dot{\gamma}_p \hat{\mathbf{n}} \tag{24}$$

and

$$\dot{\gamma} = \dot{\gamma}_y + \dot{\gamma}_b \tag{25}$$

The parameters with a subindex y are associated with the yield surface, whereas the parameters with a subindex b are associated to the rest of the infinite hardening surfaces. Again, Equations (14b) and (23) lead to the definition of hardening compliance tensors $\mathbb{H}_y^{-1}$ and $\bar{\mathbb{H}}_p^{-1}$ associated to each strain-like internal variables tensor:

$$\dot{\psi}_\xi = \dot{\psi}_{\xi_y} + \int_{p^{\mathrm{e}}}^{\bar{p}} \dot{\psi}_{\xi_p} \, \mathrm{d}p \simeq \frac{1}{2}(\dot{\boldsymbol{\alpha}} : \mathbb{H}_y^{-1} : \dot{\boldsymbol{\alpha}}) + \int_{p^{\mathrm{e}}}^{\bar{p}} \frac{1}{2}(\dot{\boldsymbol{\alpha}} : \bar{\mathbb{H}}_p^{-1} : \dot{\boldsymbol{\alpha}}) \, \mathrm{d}p \tag{26}$$

$$= \frac{1}{2}(\dot{\boldsymbol{\alpha}} : \mathbb{H}_y^{-1} : \dot{\boldsymbol{\alpha}}) + \int_{p^{\mathrm{e}}}^{\bar{p}} \frac{1}{2}(\dot{\boldsymbol{\alpha}}_p : \mathbb{H}_p^{-1} : \dot{\boldsymbol{\alpha}}_p) \, \mathrm{d}p \tag{27}$$

such that

$$\dot{\boldsymbol{\xi}}_y = -\mathbb{H}_y^{-1} : \dot{\boldsymbol{\alpha}}, \quad \dot{\boldsymbol{\xi}}_b = \int_{p^{\mathrm{e}}}^{\bar{p}} \dot{\boldsymbol{\xi}}_p \, \mathrm{d}p = -\int_{p^{\mathrm{e}}}^{\bar{p}} (\bar{\mathbb{H}}_p^{-1} : \dot{\boldsymbol{\alpha}}) \, \mathrm{d}p = -\int_{p^{\mathrm{e}}}^{\bar{p}} (\mathbb{H}_p^{-1} : \dot{\boldsymbol{\alpha}}_p) \, \mathrm{d}p \tag{28}$$

where $\bar{\mathbb{H}}_p^{-1}(p)$ is the compliance tensor for the surface defined by p, $\boldsymbol{\alpha}_p$ is the back-stress tensor of that surface and $\mathbb{H}_p^{-1}$ is an intrinsic hardening compliance tensor of surface p. The upper limit of the integral $\bar{p}$ is the last hardened surface. The same reasoning that yield (19), taking into account (24), yields also

$$\mathbb{H}_y^{-1} = \frac{1}{H_y}\langle \hat{\mathbf{n}} \otimes \hat{\mathbf{n}} \rangle, \quad \mathbb{H}_p^{-1} = \frac{1}{H_p}\langle \hat{\mathbf{n}} \otimes \hat{\mathbf{n}} \rangle, \quad \bar{\mathbb{H}}_p^{-1} = \frac{1}{\bar{H}_p}\langle \hat{\mathbf{n}} \otimes \hat{\mathbf{n}} \rangle \quad \text{with } H_y, H_p, \bar{H}_p > 0 \tag{29}$$

For the case of proportional loading, $\dot{\boldsymbol{\alpha}} = \|\dot{\boldsymbol{\alpha}}\|\hat{\mathbf{n}}$ and $\dot{\boldsymbol{\alpha}}_p = \|\dot{\boldsymbol{\alpha}}_p\|\hat{\mathbf{n}} = \|\dot{\boldsymbol{\alpha}}\|\hat{\mathbf{n}}$, so the effective hardening modulus is

$$\frac{1}{\bar{H}} = \frac{1}{H_y} + \int_{p^e}^{\bar{p}} \frac{1}{\bar{H}_p(p)}\,\mathrm{d}p = \frac{1}{H_y} + \int_{p^e}^{\bar{p}} \frac{1}{H_p(p)}\,\mathrm{d}p \tag{30}$$

as one would expect.

In the case of non-proportional loading, Prager's rule is still invoked, so $\dot{\boldsymbol{\alpha}} = \|\dot{\boldsymbol{\alpha}}\|\hat{\mathbf{n}}$ and

$$\dot{\boldsymbol{\xi}}_y = -\mathbb{H}_y^{-1} : \dot{\boldsymbol{\alpha}} \tag{31a}$$

$$= -\frac{\|\dot{\boldsymbol{\alpha}}\|}{H_y}\langle \hat{\mathbf{n}} \otimes \hat{\mathbf{n}} \rangle : \hat{\mathbf{n}} \tag{31b}$$

$$= -\frac{\|\dot{\boldsymbol{\alpha}}\|}{H_y}\hat{\mathbf{n}} \tag{31c}$$

Using Equation (24a) one obtains

$$\dot{\gamma}_y = \frac{\|\dot{\boldsymbol{\alpha}}\|}{H_y} \tag{32}$$

But in non-proportional loading the hardening rule for the hardening surfaces is a different one, for example $\dot{\boldsymbol{\alpha}}_p = \|\dot{\boldsymbol{\alpha}}_p\|\hat{\mathbf{m}}$ (with $\hat{\mathbf{m}} \neq \hat{\mathbf{n}}$ given by the normal to both surfaces at the contact point). Thus,

$$\begin{aligned} \dot{\boldsymbol{\xi}}_p &= -\mathbb{H}_p^{-1} : \dot{\boldsymbol{\alpha}}_p \\ &= -\frac{\|\dot{\boldsymbol{\alpha}}_p\|}{H_p}\langle \hat{\mathbf{n}} \otimes \hat{\mathbf{n}} \rangle : \hat{\mathbf{m}} \\ &= -\frac{\|\dot{\boldsymbol{\alpha}}_p\|\langle \hat{\mathbf{m}} : \hat{\mathbf{n}} \rangle}{H_p}\hat{\mathbf{n}} \end{aligned} \tag{33}$$

In this case, if $\langle \hat{\mathbf{m}} : \hat{\mathbf{n}} \rangle \neq 0$ the surfaces keep in contact if they are already in contact and

$$\frac{\mathrm{d}}{\mathrm{d}t}(\|\boldsymbol{\alpha} - \boldsymbol{\alpha}_p\|) = 0 \Rightarrow \hat{\mathbf{m}} : (\dot{\boldsymbol{\alpha}} - \dot{\boldsymbol{\alpha}}_p) = 0 \Rightarrow \|\dot{\boldsymbol{\alpha}}_p\| = \|\dot{\boldsymbol{\alpha}}\|\langle \hat{\mathbf{m}} : \hat{\mathbf{n}} \rangle \tag{34}$$

where the bracket function is introduced to force $\|\dot{\boldsymbol{\alpha}}_p\| = 0$ when $\hat{\mathbf{m}} : \hat{\mathbf{n}} < 0$ (the yield surface moves towards inside the hardening one). This equation may be considered a 'consistency equation' for the hardening surfaces. In consequence, Equation (33) may be written as

$$\dot{\boldsymbol{\xi}}_p = -\frac{\|\dot{\boldsymbol{\alpha}}\| \langle \hat{\mathbf{m}} : \hat{\mathbf{n}} \rangle^2}{H_p} \hat{\mathbf{n}} \tag{35}$$

so Equation (24b) yields

$$\dot{\gamma}_p = \frac{\|\dot{\boldsymbol{\alpha}}\| \langle \hat{\mathbf{m}} : \hat{\mathbf{n}} \rangle^2}{H_p} \tag{36}$$

Therefore, as $\dot{\gamma} = \|\dot{\boldsymbol{\alpha}}\|/H$, in non-proportional loading the effective hardening modulus is given by

$$\frac{1}{H} = \frac{1}{H_y} + \int_{p^e}^{\bar{p}} \frac{1}{\bar{H}_p} \, \mathrm{d}p = \frac{1}{H_y} + \int_{p^e}^{\bar{p}} \frac{\langle \hat{\mathbf{m}} : \hat{\mathbf{n}} \rangle^2}{H_p} \, \mathrm{d}p \tag{37}$$

and the hardening compliance tensor may be written as

$$\mathbb{H}^{-1} = \mathbb{H}_y^{-1} + \int_{p^e}^{\bar{p}} \bar{\mathbb{H}}_p^{-1} \, \mathrm{d}p = \mathbb{H}_y^{-1} + \int_{p^e}^{\bar{p}} (\mathbb{H}_p^{-1} : \mathbb{M}^!) \, \mathrm{d}p \tag{38}$$

where

$$\mathbb{M}^! = \langle \hat{\mathbf{m}} \otimes \hat{\mathbf{m}} \rangle : \langle \hat{\mathbf{n}} \otimes \hat{\mathbf{n}} \rangle \tag{39}$$

is the geometric tensor, comparable to the ones of Reference [8]. Note, for example that if $\langle \hat{\mathbf{n}} : \hat{\mathbf{m}} \rangle = 0$ the effective hardening is given solely by H_y, as one desires, since the outer surfaces are not being tracked. This defines the new homology generation, in contrast with standard bounding surface plasticity which is commanded by $\langle \hat{\mathbf{n}} : \dot{\boldsymbol{\varepsilon}} \rangle$. Now, 'unloading' and 'new homology' are different events. The tensor $\boldsymbol{\sigma}_0$ would be better termed 'reference' stress tensor, although we will keep the standard terminology.

It can be seen from the previous developments that the current model is nothing different from classical J_2-plasticity, since all the tools enter in the formulation only through the effective hardening modulus given by Equation (38) as nonlinear kinematic hardening. In fact, Equations (21) and (22) do not differ from those of classical associative kinematically hardened plasticity (see Reference [24]).

4. COMPARISON WITH MULTILAYER PLASTICITY USING PRAGER'S TRANSLATION RULE

The model presented here follows the bounding surface plasticity philosophy to model the non-linear kinematic hardening of classical J_2-plasticity, just as the model of Reference [8] does with multilayer plasticity. Actually, during the development of the model we have invoked the existence of an infinite number of surfaces being tracked and therefore, a comparison between both models is expedient.

As can be seen in this paper and in Reference [8], both models are developed directly from the associative plasticity, both in hardening and flow rule. All the equations until the split of the internal strain-like variables are coincident. At this point, multilayer plasticity yields

$$\boldsymbol{\xi} = \boldsymbol{\xi}^1 + \sum_{i=2}^{a} \boldsymbol{\xi}^i \tag{40}$$

where a is the number of moving surfaces (including the yield surface), whereas the model herein developed, as a consequence of the infinite number of surfaces, yields

$$\boldsymbol{\xi} = \boldsymbol{\xi}_y + \int_{p^e}^{\bar{p}} \boldsymbol{\xi}_p \, \mathrm{d}p \tag{41}$$

Similar comparisons may be developed for Equations (25)–(38).

For Equation (39) the situation is different because of two reasons. The first one is that Equation (31) of Reference [8] is incorrect if assumption (19) is to be accomplished; it lacks the tensor $\langle \hat{\mathbf{m}}^1 \otimes \hat{\mathbf{m}}^1 \rangle = \langle \hat{\mathbf{n}} \otimes \hat{\mathbf{n}} \rangle$, although this does not influence the computational results since $\mathbb{H}$ is included in the formulation only through $(\hat{\mathbf{n}} : \mathbb{H} : \hat{\mathbf{n}})$. The right equation for a hardening derived from a potential would be

$$\mathbb{M}^{i!} := \langle \hat{\mathbf{m}}^i \otimes \hat{\mathbf{m}}^i \rangle : \langle \hat{\mathbf{m}}^{i-1} \otimes \hat{\mathbf{m}}^{i-1} \rangle : \cdots : \langle \hat{\mathbf{m}}^2 \otimes \hat{\mathbf{m}}^2 \rangle : \langle \hat{\mathbf{n}} \otimes \hat{\mathbf{n}} \rangle \tag{42}$$

This way, $\mathbb{H}$ fulfils hypothesis (19) and still gives the same result.

The second is due to the way the surfaces are being tracked. Whereas in multilayer plasticity the inner surfaces 'push' the outer ones in a direction such that the movement of the latter ones is the minimum possible, in this bounding surface model this is a virtually impossible task to perform, since the number of surfaces is infinite. Therefore, it is necessary to develop a way of tracking the surfaces without the need of storing the infinite number of back-stresses for them. The way to do this is to force all the surfaces inside the 'active' one to be in contact at the same point in the stress-space (but not necessarily at the current stress-point), in contrast with the multilayer plasticity model of Reference [8] where the surfaces are in contact at different points. In consequence, in the latter each surface has an associated $\hat{\mathbf{m}}^i$ tensor defining the direction of that contact point in the stress space, while in the former there is only one $\hat{\mathbf{m}}$ for all the surfaces. In both models $\mathbb{M}^{i!}$ or $\mathbb{M}^{!}$ transfers the hardening tensor of surface i to the hardening direction given by Prager's rule, but whereas in the mentioned multilayer model this implies to go over all the directions of the surfaces inside i as in Equation (42), in bounding surface plasticity this implies to go over only $\hat{\mathbf{m}}$ and $\hat{\mathbf{n}}$, as Equation (39) shows. Nonetheless, the algorithmic discrete implementation will force another direction to be included in the algorithmic $\mathbb{M}^{!}$ tensor.

5. IMPLICIT ALGORITHM

In this section we develop a fully implicit backward-Euler algorithm for the model amenable of consistent linearization in order to keep the asymptotic quadratic convergence of the Newton–Raphson algorithms in a typical finite element program.

As a matter of notation, $(\cdot)_{n+1}$ will denote approximations for the values for the unconverged step $n+1$ at the current iteration. The iteration index will be omitted for convenience of

notation except when noted. $(\cdot)_n$ will denote the values at converged step n, whereas $\Delta(\cdot)$ denotes the increment $(\cdot)_{n+1} - (\cdot)_n$ for the current iteration.

The yield function equation, to be enforced at 'time' step $n+1$, is

$$f_{n+1} := \|\boldsymbol{\sigma}_{n+1} - \boldsymbol{\alpha}_{n+1}\| - r = 0 \tag{43}$$

The stress tensor is obtained from

$$\boldsymbol{\sigma}_{n+1} = \boldsymbol{\sigma}_n + 2\mu\Delta\boldsymbol{\varepsilon} \tag{44a}$$

$$= \boldsymbol{\sigma}_n + 2\mu\Delta\boldsymbol{\varepsilon}^{\mathrm{e}} - 2\mu\Delta\boldsymbol{\varepsilon}^{\mathrm{p}} \tag{44b}$$

where $\boldsymbol{\sigma}^{\mathrm{tr}}_{n+1} := \boldsymbol{\sigma}_n + 2\mu\Delta\boldsymbol{\varepsilon}^{\mathrm{e}}$ is usually named 'trial stress tensor' or 'elastic predictor stress tensor' and $2\mu\Delta\boldsymbol{\varepsilon}^{\mathrm{p}}$ is named 'plastic corrector of the stress tensor'; see for example Reference [1] for a background. The associative flow and hardening rules, evaluated also at the end of the step, are

$$\Delta\boldsymbol{\varepsilon}^{\mathrm{p}} = \Delta\gamma\,\frac{\partial f_{n+1}}{\partial\boldsymbol{\sigma}_{n+1}} = \Delta\gamma\hat{\mathbf{n}}_{n+1} \tag{45}$$

$$\Delta\boldsymbol{\xi} = \Delta\gamma\,\frac{\partial f_{n+1}}{\partial\boldsymbol{\alpha}_{n+1}} = -\Delta\gamma\hat{\mathbf{n}}_{n+1} \tag{46}$$

Thus, the stress and back-stress tensors are given by

$$\boldsymbol{\sigma}_{n+1} = \boldsymbol{\sigma}^{\mathrm{tr}}_{n+1} - 2\mu\Delta\gamma\hat{\mathbf{n}}_{n+1} \tag{47}$$

$$\Delta\boldsymbol{\alpha} = -\mathbb{H}_{n+1} : \Delta\boldsymbol{\xi} = H_{n+1}\Delta\gamma\hat{\mathbf{n}}_{n+1} \tag{48}$$

since $\mathbb{H}_{n+1} = H_{n+1}\langle\hat{\mathbf{n}}_{n+1}\otimes\hat{\mathbf{n}}_{n+1}\rangle$. As a consequence, the direction for the return and the translation of the yield surface is completely determined from the trial state as it can be easily seen. Since $(\boldsymbol{\sigma}_{n+1} - \boldsymbol{\alpha}_{n+1})$ has the direction $\hat{\mathbf{n}}_{n+1}$, one can write

$$\|\boldsymbol{\sigma}_{n+1} - \boldsymbol{\alpha}_{n+1}\|\hat{\mathbf{n}}_{n+1} = \boldsymbol{\sigma}^{\mathrm{tr}}_{n+1} - 2\mu\Delta\gamma\hat{\mathbf{n}}_{n+1} - \boldsymbol{\alpha}_n - \bar{H}_{n+1}\Delta\gamma\hat{\mathbf{n}}_{n+1} \tag{49}$$

and therefore the tensor $\boldsymbol{\sigma}^{\mathrm{tr}}_{n+1} - \boldsymbol{\alpha}_n$ has to be also in the direction of $\hat{\mathbf{n}}_{n+1}$, so the unitary direction is

$$\hat{\mathbf{n}}_{n+1} = \frac{\mathbf{n}^{\mathrm{tr}}_{n+1}}{\|\mathbf{n}^{\mathrm{tr}}_{n+1}\|} \quad \text{with } \mathbf{n}^{\mathrm{tr}}_{n+1} := \boldsymbol{\sigma}^{\mathrm{tr}}_{n+1} - \boldsymbol{\alpha}_n \tag{50}$$

The discrete counterparts of Equations (31c) and (35) for a backward-Euler algorithm are, respectively,

$$\Delta\boldsymbol{\xi}_y = -\mathbb{H}^{-1}_{y,n+1} : \Delta\boldsymbol{\alpha} = -\frac{\langle\hat{\mathbf{n}}_{n+1} : \Delta\boldsymbol{\alpha}\rangle}{H_y}\,\hat{\mathbf{n}}_{n+1} \tag{51}$$

and

$$\Delta\boldsymbol{\xi}_p = -\mathbb{H}^{-1}_{p,n+1} : \Delta\boldsymbol{\alpha}_p = -\frac{\langle \hat{\mathbf{m}}_{n+1} : \hat{\mathbf{n}}_{n+1}\rangle \langle \hat{\mathbf{m}}_{n+1} : \Delta\boldsymbol{\alpha}_p\rangle}{H_p}\, \hat{\mathbf{n}}_{n+1} \tag{52}$$

since in a similar way $\mathbb{H}_{y,n+1} = H_y \langle \hat{\mathbf{n}}_{n+1} \otimes \hat{\mathbf{n}}_{n+1}\rangle$ and $\mathbb{H}_{p,n+1} = H_p \langle \hat{\mathbf{n}}_{n+1} \otimes \hat{\mathbf{n}}_{n+1}\rangle$ (note that H_y and H_p are constant).

Equations (33) and (52) do not look similar because the consistency equation for the hardening surfaces (34) is different for the discrete case. Generally, $\Delta\boldsymbol{\alpha}_p$ will not be in the direction of $\hat{\mathbf{m}}_{n+1}$, and therefore, an $\Delta\boldsymbol{\alpha}_p$ in a different direction will imply in the contact direction a translation of $(\Delta\boldsymbol{\alpha}_p : \hat{\mathbf{m}}_{n+1})$. In consequence, Equation (34) reads now

$$\frac{\mathrm{d}}{\mathrm{d}t}(\|\boldsymbol{\alpha} - \boldsymbol{\alpha}_p\|) = 0 \;\Rightarrow\; \hat{\mathbf{m}}_{n+1} : \Delta\boldsymbol{\alpha} - \hat{\mathbf{m}}_{n+1} : \Delta\boldsymbol{\alpha}_p = 0 \;\Rightarrow\; \|\Delta\boldsymbol{\alpha}\| \langle \hat{\mathbf{m}}_{n+1} : \hat{\mathbf{n}}_{n+1}\rangle = \langle \Delta\boldsymbol{\alpha}_p : \hat{\mathbf{m}}_{n+1}\rangle \tag{53}$$

which yields (52) (the Macauley bracket is introduced to account for the absence of hardening when $\hat{\mathbf{m}}_{n+1} : \Delta\boldsymbol{\alpha}_p < 0$). Geometrically speaking, defining $\hat{\boldsymbol{\alpha}}_p = \Delta\boldsymbol{\alpha}_p / \|\Delta\boldsymbol{\alpha}_p\|$, the algorithmic treatment of (35) (that is to say, the usage of (52)) avoids the possible lack of convergence when $\hat{\mathbf{n}}_{n+1} : \hat{\boldsymbol{\alpha}}_p < 0$ and the surface hardens. As a consequence, the algorithmic geometric tensor (39) for surface p is

$$\mathbb{M}^{!alg}_p = \langle \hat{\mathbf{m}}_{n+1} \otimes \hat{\mathbf{m}}_{n+1}\rangle : \langle \hat{\boldsymbol{\alpha}}_p \otimes \hat{\mathbf{m}}_{n+1}\rangle : \langle \hat{\mathbf{n}}_{n+1} \otimes \hat{\mathbf{n}}_{n+1}\rangle \tag{54}$$

As in multilayer plasticity, there is a geometric algorithmic tensor for every surface.

If the final position of the yield surface is known (it depends on the consistency parameter to be obtained later), the discrete hardening direction of the hardening surfaces may be determined from the final position of those surfaces. This position is given by the condition that the surfaces do not overlap with the yield one (see Figures 3 and 4):

$$\boldsymbol{\alpha}_{p,n+1} = \boldsymbol{\alpha}_{n+1} + (r - pR)\hat{\mathbf{m}}_{n+1} \quad \text{with} \;\; p \leqslant p_{n+1} \tag{55}$$

where

$$\hat{\mathbf{m}}_{n+1} := \frac{\mathbf{m}_{n+1}}{\|\mathbf{m}_{n+1}\|} \quad \text{with} \;\; \mathbf{m}_{n+1} := \boldsymbol{\alpha}_{n+1} - \boldsymbol{\alpha}_{b,n+1} \neq \mathbf{0} \quad \text{for plastic step} \tag{56}$$

and in which

$$\boldsymbol{\alpha}_{b,n+1} = \boldsymbol{\sigma}_{0b,n+1} + p_{n+1}(\boldsymbol{\beta}_{b,n+1} - \boldsymbol{\sigma}_{0b,n+1}) \tag{57}$$

is the back-stress of the smallest hardening surface that does not harden during the step and p_{n+1} is its normalized radius. The subindex b implies in this case values for $p = p_{n+1}$. Those values are computed with the trial (frozen) $\boldsymbol{\sigma}_{0b,n+1}$ and $\boldsymbol{\beta}_{b,n+1}$ if a hardening for the bounding surface is allowed for.

Let p_n be the normalized radius of the smallest hardening surface in contact with the yield surface at time-step n. For the hardening surfaces with normalized radii p such that $p_n < p \leqslant p_{n+1}$, the back-stress tensors at time-step n are given by the homology as

$$\boldsymbol{\alpha}_{p,n} = \boldsymbol{\sigma}_{0p,n} + p(\boldsymbol{\beta}_{p,n} - \boldsymbol{\sigma}_{0p,n}) \tag{58}$$

where $\boldsymbol{\sigma}_{0p,n}$ and $\boldsymbol{\beta}_{p,n}$ are the 'unloading'-stress and bounding surface back-stress tensors associated with surface p at the end of time step n. On the other hand, if $p^{\mathrm{e}} < p \leqslant p_n$ the back-stress tensors for the hardening surfaces are

$$\boldsymbol{\alpha}_{p,n} = \boldsymbol{\alpha}_n + (r - pR)\hat{\mathbf{m}}_n \tag{59}$$

where the contact stress direction tensor at time step n is

$$\hat{\mathbf{m}}_n := \frac{\mathbf{m}_n}{\|\mathbf{m}_n\|} \quad \text{with } \mathbf{m}_n := \boldsymbol{\alpha}_n - \boldsymbol{\alpha}_{b,n} \tag{60}$$

and, similarly

$$\boldsymbol{\alpha}_{b,n} = \boldsymbol{\sigma}_{0b,n} - \bar{p}_n(\boldsymbol{\beta}_{b,n} - \boldsymbol{\sigma}_{0b,n}) \tag{61}$$

with $\bar{p}_n = \min(p_n, 1)$ being the bounded normalized radius of the last hardened surface at time step n (the radius saved in the convergence phase at that time step). Therefore, the increments $\Delta\boldsymbol{\alpha}_p$ may be computed as (see Figure 4)

$$\Delta\boldsymbol{\alpha}_p = \begin{cases} \Delta\boldsymbol{\alpha} + (r - pR)(\hat{\mathbf{m}}_{n+1} - \hat{\mathbf{m}}_n) & \text{if } p^{\mathrm{e}} < p \leqslant \bar{p}_n \\ \boldsymbol{\alpha}_{n+1} + (r - pR)\hat{\mathbf{m}}_{n+1} - \boldsymbol{\sigma}_{0p,n} - p(\boldsymbol{\beta}_{p,n} - \boldsymbol{\sigma}_{0p,n}) & \text{if } \bar{p}_n < p \leqslant \bar{p}_{n+1} \\ \mathbf{0} & \text{if } p > \bar{p}_{n+1} \end{cases} \tag{62}$$

where $\bar{p}_{n+1} := \min(p_{n+1}, 1)$. The consistency parameter may be computed from

$$\Delta\boldsymbol{\xi} = -\Delta\gamma\hat{\mathbf{n}}_{n+1} \tag{63a}$$

$$= \Delta\boldsymbol{\xi}_y + \int_{p^{\mathrm{e}}}^{\bar{p}_{n+1}} \Delta\boldsymbol{\xi}_p \, \mathrm{d}p \tag{63b}$$

$$= -\Delta\gamma_y\hat{\mathbf{n}}_{n+1} - \int_{p^{\mathrm{e}}}^{\bar{p}_{n+1}} \Delta\gamma_p\hat{\mathbf{n}}_{n+1} \, \mathrm{d}p \tag{63c}$$

and Equations (51), (52) as

$$\Delta\gamma = \Delta\gamma_y + \int_{p^{\mathrm{e}}}^{\bar{p}_{n+1}} \Delta\gamma_p \, \mathrm{d}p = \frac{\|\Delta\boldsymbol{\alpha}\|}{H_y} + \int_{p^{\mathrm{e}}}^{\bar{p}_{n+1}} \frac{\langle\hat{\mathbf{n}}_{n+1} : \hat{\mathbf{m}}_{n+1}\rangle\langle\hat{\mathbf{m}}_{n+1} : \Delta\boldsymbol{\alpha}_p\rangle}{H_p} \, \mathrm{d}p \tag{64}$$

To obtain $\Delta\gamma$ it is necessary to compute $\|\Delta\boldsymbol{\alpha}\|$. To do so, since the smallest hardening surface (or 'virtual hardening surface' if $p_{n+1} > 1$) in contact with the yield surface at time-step $n+1$ has a radius of $p_{n+1}R$ and a back-stress tensor $\boldsymbol{\alpha}_{b,n+1}$, the following equation has to be fulfilled:

$$\|\boldsymbol{\alpha}_{n+1} - \boldsymbol{\alpha}_{b,n+1}\|^2 = (p_{n+1}R - r)^2 \tag{65}$$

Using Prager's translation rule

$$\boldsymbol{\alpha}_{n+1} = \boldsymbol{\alpha}_n + \Delta\lambda\hat{\mathbf{n}}_{n+1} \tag{66}$$

the previous equation reads

$$(\boldsymbol{\alpha}_n + \Delta\lambda\hat{\mathbf{n}}_{n+1} - \boldsymbol{\alpha}_{b,n+1}) : (\boldsymbol{\alpha}_n + \Delta\lambda\hat{\mathbf{n}}_{n+1} - \boldsymbol{\alpha}_{b,n+1}) = (p_{n+1}R - r)^2 \tag{67}$$

The parameter $\Delta\lambda > 0$ may be factored-out as

$$\Delta\lambda = -\bar{b} + \sqrt{\bar{b}^2 - \bar{c}} \tag{68}$$

with

$$\bar{b} := \hat{\mathbf{n}}_{n+1} : (\boldsymbol{\alpha}_n - \boldsymbol{\alpha}_{b,n+1})$$

$$\bar{c} := \|\boldsymbol{\alpha}_n - \boldsymbol{\alpha}_{b,n+1}\|^2 - (p_{n+1} - p^{\mathrm{e}})^2 R^2$$

and the consistency parameter determined from Equations (64) and (66) as

$$\Delta\gamma = \Delta\gamma_y + \int_{p^{\mathrm{e}}}^{\bar{p}_{n+1}} \Delta\gamma_p \, \mathrm{d}p = \frac{\Delta\lambda}{H_y} + \int_{p^{\mathrm{e}}}^{\bar{p}_{n+1}} \frac{\langle \hat{\mathbf{n}}_{n+1} : \hat{\mathbf{m}}_{n+1} \rangle \langle \hat{\mathbf{m}}_{n+1} : \Delta\boldsymbol{\alpha}_p(\Delta\lambda) \rangle}{H_p} \, \mathrm{d}p \tag{69}$$

Up to this point, it has been assumed that the parameter p_{n+1} was known, but it is not, since it depends on the consistency parameter increment $\Delta\gamma$. Therefore, apart from Equation (69), it is necessary to use the consistency condition that, by Equations (43), (44b) and (66) is

$$\hat{\mathbf{n}}_{n+1} : (\boldsymbol{\sigma}_{n+1}^{\mathrm{tr}} - 2\mu\Delta\gamma\hat{\mathbf{n}}_{n+1} - \boldsymbol{\alpha}_n - \Delta\lambda\hat{\mathbf{n}}_{n+1}) - r = 0 \tag{70}$$

and from which, again, the consistency parameter may be factored out as

$$\Delta\gamma = \frac{\|\mathbf{n}_{n+1}^{\mathrm{tr}}\| - \Delta\lambda - r}{2\mu} \tag{71}$$

To obtain the final value of $\Delta\gamma$ and p_{n+1}, an iterative process around p_{n+1} is employed. Denoting by the superindex i the current iteration, once the guess p_{n+1}^i is established (for example, $p_{n+1}^1 = \bar{p}_n$), the 'error' as a difference between the consistency parameters obtained by means of Equations (69) and (71) is minimized:

$$\begin{aligned} Error^i &= \Delta\gamma^{i,1} - \Delta\gamma^{i,2} \\ &= \left[\frac{\|\mathbf{n}_{n+1}^{\mathrm{tr}}\| - \Delta\lambda - r}{2\mu}\right] - \left[\frac{\Delta\lambda}{H_y} + \int_{p^{\mathrm{e}}}^{\bar{p}_{n+1}} \frac{\langle \hat{\mathbf{n}}_{n+1} : \hat{\mathbf{m}}_{n+1} \rangle \langle \hat{\mathbf{m}}_{n+1} : \Delta\boldsymbol{\alpha}_p \rangle}{H_p(p)} \, \mathrm{d}p\right] \end{aligned} \tag{72}$$

where $\Delta\lambda(p_{n+1}^i)$ is obtained from Equation (68).

5.1. Numerical integration of the constitutive equation for the plastic internal variables

To evaluate $Error^i$ through Equation (72) it is necessary to perform the integral of the second term of the right-hand side. The typical uniaxial hardening functions employed for

$$\frac{1}{H_b(p_{n+1})} = \int_{p^{\mathrm{e}}}^{\bar{p}_{n+1}} \frac{\mathrm{d}p}{H_p(p)} \tag{73}$$

are, for example, generic exponential functions of the type (see for instance References [14, 17, 21]):

$$H_b(p)=h\left(\frac{1}{\tilde{p}}-1\right)^m \;\Rightarrow\; H_p(p)=\frac{h}{m}\tilde{p}^2\left(\frac{1}{\tilde{p}}-1\right)^{m+1} \tag{74}$$

where $\tilde{p}:=(p-p^{\mathrm{e}})/(1-p^{\mathrm{e}})\not>1$ and h, m are the exponential function parameters to be obtained from two points of the shear moduli degradation curves (or alternatively from two points of the uniaxial stress–strain plots). Again, these moduli already include the $\frac{2}{3}$ factor of the uniaxial comparison. The derivative of them with respect to the basic parameter p is

$$\frac{\mathrm{d}H_p}{\mathrm{d}p}=-\frac{h}{m}\left(\frac{1}{\tilde{p}}-1\right)^m\frac{(m-1+2\tilde{p})}{(1-p^{\mathrm{e}})} \tag{75}$$

The primitive of the inverse of Equation (74b) is usually known, but the primitive of, for example, the generic $p/H_p(p)$ in explicit form, present in Equation (69) or in the ulterior needed derivatives, is usually not known. Therefore, to employ a generic algorithm it is necessary to integrate numerically Equation (69), at least for the terms which primitive may not be explicitly known. It is important to specify here the rule employed, since it is necessary to know it in order to obtain consistently linearized algorithms, both internal (at the stress-point level) and external (at the structure level).

In this paper all the terms in Equation (69) are integrated numerically. The chosen rule is the composite Simpson's one, because it shows a good balance between accuracy and simplicity, see for example Reference [23]. In this rule, for example

$$\Delta\gamma_b(p_{n+1})=\int_{p^{\mathrm{e}}}^{\bar{p}_{n+1}}\Delta\gamma_p(p)\,\mathrm{d}p \tag{76}$$

$$\simeq\frac{h}{3}[\Delta\gamma_p(p^{\mathrm{e}})+4\Delta\gamma_p(p^{\mathrm{e}}+h)+2\Delta\gamma_p(p^{\mathrm{e}}+2h)+4\Delta\gamma_p(p^{\mathrm{e}}+3h)$$
$$+\cdots+2\Delta\gamma_p(p_{n+1}-2h)+4\Delta\gamma_p(p_{n+1}-h)+\Delta\gamma_p(p_{n+1})] \tag{77}$$

where $h:=(\bar{p}_{n+1}-p^{\mathrm{e}})/2n$ and $2n$ is the number of equally spaced subintervals with which the integral is evaluated fitting a parabola in every two ones. For convenience, since it will be employed extensively, define a composite Simpson operator for $2n+1$ points ($2n$ intervals) with the variable p varying from p^{e} to $\bar{p}_{n+1}$ as

$$\mathscr{S}_{2n}\{\cdot\}_{p^{\mathrm{e}}}^{\bar{p}_{n+1}}:=\frac{h}{3}\left\{(\cdot)_{p=p^{\mathrm{e}}}+\sum_{\eta=1}^{n-1}[4(\cdot)_{p=p^{\mathrm{e}}+(2\eta-1)h}+2(\cdot)_{p=p^{\mathrm{e}}+2\eta h}]+4(\cdot)_{p=\bar{p}_{n+1}-h}+(\cdot)_{p=\bar{p}_{n+1}}\right\} \tag{78}$$

With this notation, Equation (77) may be written succinctly as

$$\Delta\gamma_b(p_{n+1})\simeq\mathscr{S}_{2n}\{\Delta\gamma_p\}_{p^{\mathrm{e}}}^{\bar{p}_{n+1}} \tag{79}$$

As is straightforward to prove, this operator is a linear operator in the sense that given c_1, c_2 constants and $\mathscr{F}, \mathscr{G}$ functions of p:

$$\mathscr{S}_{2n}\{c_1\mathscr{F} + c_2\mathscr{G}\}_{p^e}^{\bar{p}_{n+1}} = c_1\mathscr{S}_{2n}\{\mathscr{F}\}_{p^e}^{\bar{p}_{n+1}} + c_2\mathscr{S}_{2n}\{\mathscr{G}\}_{p^e}^{\bar{p}_{n+1}} \tag{80}$$

This property will be used to obtain computationally efficient expressions.

Aside, given the chosen integration scheme with sampling points varying with p_{n+1}, in the case that between p_n and p_{n+1} there is a memory surface it is necessary to split the integration into several sums, each one corresponding to the interval between two p^i, being p^i the normalized radii of the memory surfaces or any of p_n, p_{n+1}. The variation will allow global convergence to happen even in this case. In consequence, if there are s memory surfaces, Equation (79) may be written as

$$\Delta\gamma_b(p_{n+1}) \simeq \sum_{i=1}^{s} \mathscr{S}_{2n}\{\Delta\gamma_p\}_{p^{i-1}}^{p^i} + \mathscr{S}_{2n}\{\Delta\gamma_p\}_{p^s}^{\bar{p}_{n+1}} \tag{81}$$

being $p^0 := p^e$. This expression includes (79) by setting $s = 0$. The scheme may be used even if there is no crossing of surfaces since p_n is constant and, therefore, may be treated as a memory surface. To simplify notation even further, we will denote (81) by

$$\Delta\gamma_b(p_{n+1}) \simeq \sum_{i=1}^{s,\bar{p}_{n+1}} \mathscr{S}_{2n}\{\Delta\gamma_p\}_{p^{i-1}}^{p^i} \tag{82}$$

5.2. *Inclusion of a kinematic hardening for the bounding surface*

On occasions it is desirable to include a kinematic hardening for the bounding surface in order to allow for a maximum degradation of the constitutive tangent (both for physical and numerical reasons) or in order to allow for stresses outside the surface. This is simply done by using a hardening function that is non-zero at the bounding surface (adding a H_0); see for example Reference [21]:

$$\begin{aligned} H_b &= h\left(\frac{1}{\tilde{p}} - 1\right)^m + H_0 \\ \Rightarrow H_p(p) &= \frac{h}{m}\,\tilde{p}^2\left(\frac{1}{\tilde{p}} - 1\right)^{m+1} + \frac{2H_0}{m}\,\tilde{p}^2\left(\frac{1}{\tilde{p}} - 1\right) + \frac{H_0^2}{hm}\,\tilde{p}^2\left(\frac{1}{\tilde{p}} - 1\right)^{1-m} \end{aligned} \tag{83}$$

This inclusion is the reason for allowing $p_{n+1} > 1$ and the usage of a bounded $\bar{p}_{n+1}$ in the previous developments.

Owing to this kinematic hardening, the uniaxial effective hardening when the bounding surface is reached is given by $(H_y^{-1} + H_0^{-1})^{-1}$. Thus, if μ^* is the desired minimum ratio between the effective tangent shear modulus and the initial one, H_0 may be readily determined by

$$H_0 = \frac{2\mu}{1/\mu^* - 1 + 2\mu/H_y} \tag{84}$$

5.3. Computation of $\boldsymbol{\beta}_{p,n}, \boldsymbol{\sigma}_{0p,n}, \boldsymbol{\beta}_{b,n+1}, \boldsymbol{\sigma}_{0b,n+1}$

In Equations (57) and (58) there is a need for the knowledge of $\boldsymbol{\beta}_{p,n}$, $\boldsymbol{\sigma}_{0p,n}$, $\boldsymbol{\beta}_{b,n+1}$ and $\boldsymbol{\sigma}_{0b,n+1}$. Nonetheless, to store all these values in memory would be expensive. Fortunately, the values of the $\boldsymbol{\beta}_p$ tensors that describe the positions of the virtual surface may be obtained from the back-stress tensors of the memory surfaces $\boldsymbol{\alpha}^i$. Between stored surfaces i and $i+1$ of radii $\bar{p}^i R$ and $\bar{p}^{i+1} R$, the tensors $\boldsymbol{\beta}_{p,n}, \boldsymbol{\sigma}_{0p,n}$ may be determined from the condition that they must guarantee the continuity of the evolution of the back-stress tensor of the 'active' hardening surface (or in other words, they must avoid the overlapping of the surfaces, see Figure 4). Therefore, given

$$\boldsymbol{\alpha}^i = \boldsymbol{\sigma}_{0p,n} + \bar{p}^i(\boldsymbol{\beta}_{p,n} - \boldsymbol{\sigma}_{0p,n}), \quad \boldsymbol{\alpha}^{i+1} = \boldsymbol{\sigma}_{0p,n} + \bar{p}^{i+1}(\boldsymbol{\beta}_{p,n} - \boldsymbol{\sigma}_{0p,n}) \tag{85}$$

the 'unload' stress tensor and back-stress of the bounding surface may be solved for as

$$\boldsymbol{\sigma}_{0p,n} = \frac{\bar{p}^{i+1}}{\bar{p}^{i+1} - \bar{p}^i}\,\boldsymbol{\alpha}^i - \frac{\bar{p}^i}{\bar{p}^{i+1} - \bar{p}^i}\,\boldsymbol{\alpha}^{i+1} \tag{86}$$

$$\boldsymbol{\beta}_{p,n} = \frac{\bar{p}^{i+1} - 1}{\bar{p}^{i+1} - \bar{p}^i}\,\boldsymbol{\alpha}^i - \frac{\bar{p}^i - 1}{\bar{p}^{i+1} - \bar{p}^i}\,\boldsymbol{\alpha}^{i+1} \quad \text{with } \bar{p}^{i+1} < p < \bar{p}^i \tag{87}$$

In the previous expressions $\bar{p}^{u+1} := p^{\mathrm{e}}$ and $\bar{p}^0 = 1$, being u the index of the last stored surface, whereas $\boldsymbol{\alpha}^{u+1} = \boldsymbol{\alpha}$ and $\boldsymbol{\alpha}^0 = \boldsymbol{\beta}_{b,n} = \boldsymbol{\sigma}_{0b,n}$ (which may be different from zero if there has been hardening of the bounding surface).

5.4. Tangent for the internal iterative process

To reach a solution for p_{n+1} a Newton–Raphson algorithm is employed. To obtain quadratic convergence, it is necessary to linearize $Error^i$. Omitting the iteration index:

$$\frac{\partial Error}{\partial p_{n+1}} = \frac{\partial \Delta\gamma^1}{\partial p_{n+1}} - \frac{\partial \Delta\gamma^2}{\partial p_{n+1}} \tag{88}$$

Since both $\Delta\gamma^1$ and $\Delta\gamma^2$ depend on $\Delta\lambda$, it is necessary to obtain $\partial\Delta\lambda/\partial p_{n+1}$. From Equation (67), using Equation (57):

$$\Delta\lambda\,\frac{\partial\Delta\lambda}{\partial p_{n+1}} + [\hat{\mathbf{n}}_{n+1} : (\boldsymbol{\alpha}_n - \boldsymbol{\alpha}_{b,n+1})]\frac{\partial\Delta\lambda}{\partial p_{n+1}} - [\mathbf{m}_{n+1} : (\boldsymbol{\beta}_{b,n+1} - \boldsymbol{\sigma}_{0b,n+1})] - (p_{n+1}R - r)R = 0 \tag{89}$$

and factoring-out $\partial\Delta\lambda/\partial p_{n+1}$ one obtains

$$\frac{\partial\Delta\lambda}{\partial p_{n+1}} = \frac{a}{b} \tag{90}$$

where

$$a := (p_{n+1} - p^{\mathrm{e}})R^2 + \mathbf{m}_{n+1} : \mathbf{b}_{n+1} \tag{91}$$

$$b := \Delta\lambda + \hat{\mathbf{n}}_{n+1} : (\boldsymbol{\alpha}_n - \boldsymbol{\alpha}_{b,n+1}) = \Delta\lambda + \bar{b} \tag{92}$$

$$\mathbf{b}_{n+1} := \boldsymbol{\beta}_{b,n+1} - \boldsymbol{\sigma}_{0b,n+1} \quad (=\mathbf{0} \text{ if } p_{n+1} > 1) \tag{93}$$

so from Equation (71), the first term of the right-hand side of Equation (88) is computed as

$$\frac{\partial \Delta\gamma^1}{\partial p_{n+1}} = -\frac{1}{2\mu}\frac{\partial \Delta\lambda}{\partial p_{n+1}} \tag{94}$$

It is worth noticing that there may be a derivative term not included in Equation (89) associated with the change in the tensors $\boldsymbol{\beta}_{b,n+1}, \boldsymbol{\sigma}_{0b,n+1}$ if there is a new unloading memory surface respect to the previous iteration. Nonetheless, this term would become infinite since there is a jump from one value to the other (not a smooth transition) and in consequence, no term is added to take into account this effect. As a result, there may be a loss of the second order convergence from the previous iteration to the actual one, but since this will be an infrequent event if the number of memory surfaces is kept not too high, the computational significance will be minor.

To compute the second term we depart from Equation (69a) using the numerical integration given by Equation (78), and we take its p_{n+1}-derivative:

$$\frac{\partial \Delta\gamma^2}{\partial p_{n+1}} = \frac{1}{H_y}\frac{\partial \Delta\lambda}{\partial p_{n+1}} + \frac{\mathscr{H}(1-p_{n+1})}{p_{n+1}-p^s}\mathscr{S}_{2n}\{\Delta\gamma_p\}_{p^s}^{\bar{p}_{n+1}} + \sum_{i=1}^{s,\bar{p}_{n+1}} \mathscr{S}_{2n}\left\{\frac{\partial \Delta\gamma_p(p)}{\partial p_{n+1}}\right\}_{p^{i-1}}^{p^i} \tag{95}$$

where for $0 \leqslant q \leqslant 2n$, since by Equation (69b) $\Delta\gamma_p = \langle \hat{\mathbf{n}}_{n+1} : \Delta\boldsymbol{\alpha}_p \rangle / H_p$, the derivative of the consistency parameter for the surfaces is

$$\begin{aligned}
\frac{\partial \Delta\gamma_p(p)}{\partial p_{n+1}} &= \frac{\partial}{\partial p_{n+1}}\left[\frac{1}{H_p(p)}\langle \hat{\mathbf{n}}_{n+1} : \hat{\mathbf{m}}_{n+1}\rangle \langle \hat{\mathbf{n}}_{n+1} : \Delta\boldsymbol{\alpha}_p(p)\rangle\right] \\
&= -\frac{1}{H_p}\frac{\partial H_p}{\partial p}\bigg|_{p^s+qh}\frac{q}{2n}\Delta\gamma_p + \frac{\mathscr{H}(\hat{\mathbf{m}}_{n+1} : \hat{\mathbf{n}}_{n+1})}{H_p}\langle \hat{\mathbf{m}}_{n+1} : \Delta\boldsymbol{\alpha}_p\rangle\left(\hat{\mathbf{n}}_{n+1} : \frac{\partial \hat{\mathbf{m}}_{n+1}}{\partial p_{n+1}}\right) \\
&\quad + \frac{\mathscr{H}(\hat{\mathbf{m}}_{n+1} : \Delta\boldsymbol{\alpha}_p)}{H_p}\langle \hat{\mathbf{m}}_{n+1} : \hat{\mathbf{n}}_{n+1}\rangle\left(\hat{\mathbf{m}}_{n+1} : \frac{\partial \Delta\boldsymbol{\alpha}_p}{\partial p_{n+1}} + \Delta\boldsymbol{\alpha}_p : \frac{\partial \hat{\mathbf{m}}_{n+1}}{\partial p_{n+1}}\right)
\end{aligned} \tag{96}$$

for $p = p^s + qh > p^s$. For the cases $p \leqslant p^s$ or $p_{n+1} > 1$ the same expression may be used setting $\partial H_p/\partial p = 0$. The function $\mathscr{H}(x) := \frac{1}{2}(1 + x/|x|)$ is the Heaviside function. Note that in Equation (78) q may be either $q = 2\eta - 1$ or 2η. Also, $\partial H_p/\partial p_{n+1}$ is non-zero for $p > p^s$ and $p_{n+1} < 1$ since due to the numerical integration procedure the sampling point p changes as p_{n+1} does.

The expression for $\partial \Delta\boldsymbol{\alpha}_p/\partial p_{n+1}$ is obtained from Equation (62) as (recall that $r = p^e R$)

$$\frac{\partial \Delta\boldsymbol{\alpha}_p}{\partial p_{n+1}} = \frac{\partial \Delta\lambda}{\partial p_{n+1}}\hat{\mathbf{n}}_{n+1} + (r - pR)\frac{\partial \hat{\mathbf{m}}_{n+1}}{\partial p_{n+1}} - \frac{qR}{2n}\mathbf{t}_{n+1} \quad \text{with } p = p^s + qh \tag{97}$$

where

$$\mathbf{t}_{n+1}(p) := \begin{cases} \mathbf{0} & \text{if } p \leqslant p^s \\ \hat{\mathbf{m}}_{n+1} + (\boldsymbol{\beta}_{p,n} - \boldsymbol{\sigma}_{op,n})/R & \text{if } p > p^s \geqslant p_n \end{cases} \tag{98}$$

and from Equations (56), (57) and (66),

$$\frac{\partial \hat{\mathbf{m}}_{n+1}}{\partial p_{n+1}} = \frac{1}{\|\mathbf{m}_{n+1}\|} \mathbb{P}_{\mathbf{m}} : \left[\frac{\partial \Delta\lambda}{\partial p_{n+1}} \hat{\mathbf{n}}_{n+1} - (\boldsymbol{\beta}_{b,n} - \boldsymbol{\sigma}_{0b,n}) \right] \tag{99}$$

where $\mathbb{P}_{\mathbf{m}}$ is the perpendicular projector

$$\mathbb{P}_{\mathbf{m}} := \mathbb{I} - \hat{\mathbf{m}}_{n+1} \otimes \hat{\mathbf{m}}_{n+1} \tag{100}$$

and $\mathbb{I}$ is the fourth-order identity tensor.

5.5. *Algorithmic elastoplastic tangent*

To preserve the second-order convergence of the external Newton algorithm, the consistent elastoplastic tangent must be used [1, 24]. This operator is defined as

$$\mathbb{C}^{\text{ep}}_{n+1} := \frac{\partial \boldsymbol{\sigma}^{\text{f}}_{n+1}}{\partial \boldsymbol{\varepsilon}^{\text{f}}_{n+1}} \tag{101}$$

where the superscript f denotes complete tensor, including the volumetric component:

$$\boldsymbol{\varepsilon}^{\text{f}}_{n+1} = \boldsymbol{\varepsilon}_{n+1} + (\hat{\mathbf{I}} \otimes \hat{\mathbf{I}}) : \boldsymbol{\varepsilon}^{\text{f}}_{n+1} \tag{102}$$

$$\boldsymbol{\sigma}^{\text{f}}_{n+1} = \boldsymbol{\sigma}_{n+1} + 3K(\hat{\mathbf{I}} \otimes \hat{\mathbf{I}}) : \boldsymbol{\varepsilon}^{\text{f}}_{n+1} \tag{103}$$

and K is the bulk modulus. The tensor $\hat{\mathbf{I}} = \mathbf{I}/\|\mathbf{I}\|$, being $\mathbf{I}$ the second-order identity one. In consequence,

$$\mathbb{C}^{\text{ep}}_{n+1} = 3K\hat{\mathbf{I}} \otimes \hat{\mathbf{I}} + \frac{\partial \boldsymbol{\sigma}_{n+1}}{\partial \boldsymbol{\varepsilon}_{n+1}} : \mathbb{P}_{\mathbf{I}} \tag{104}$$

where $\mathbb{P}_{\mathbf{I}} = \mathbb{I} - \hat{\mathbf{I}} \otimes \hat{\mathbf{I}}$.

On the other hand, since

$$\boldsymbol{\sigma}_{n+1} = \boldsymbol{\alpha}_{n+1} + r\hat{\mathbf{n}}_{n+1} \tag{105}$$

we obtain

$$\frac{\partial \boldsymbol{\sigma}_{n+1}}{\partial \boldsymbol{\varepsilon}_{n+1}} = \frac{\partial \boldsymbol{\alpha}_{n+1}}{\partial \boldsymbol{\varepsilon}_{n+1}} + r \frac{\partial \hat{\mathbf{n}}_{n+1}}{\partial \boldsymbol{\varepsilon}_{n+1}} \tag{106}$$

From (50):

$$\frac{\partial \hat{\mathbf{n}}_{n+1}}{\partial \boldsymbol{\varepsilon}_{n+1}} = \frac{2\mu}{\|\mathbf{n}^{\text{tr}}_{n+1}\|} \mathbb{P}_{\mathbf{n}} \tag{107}$$

where $\mathbb{P}_{\mathbf{n}} = \mathbb{I} - \hat{\mathbf{n}}_{n+1} \otimes \hat{\mathbf{n}}_{n+1}$. Aside, from (66),

$$\frac{\partial \boldsymbol{\alpha}_{n+1}}{\partial \boldsymbol{\varepsilon}_{n+1}} = \hat{\mathbf{n}}_{n+1} \otimes \frac{\partial \Delta\lambda}{\partial \boldsymbol{\varepsilon}_{n+1}} + \Delta\lambda \frac{\partial \hat{\mathbf{n}}_{n+1}}{\partial \boldsymbol{\varepsilon}_{n+1}} \tag{108}$$

of which only $\partial \Delta\lambda / \partial \boldsymbol{\varepsilon}_{n+1}$ remains unknown. This tensor may be determined from the equation for $\Delta\lambda$. Taking the $\boldsymbol{\varepsilon}_{n+1}$-derivative of (67) the following expression is obtained:

$$\begin{aligned} &\Delta\lambda \frac{\partial \Delta\lambda}{\partial \boldsymbol{\varepsilon}_{n+1}} + \Delta\lambda (\boldsymbol{\alpha}_n - \boldsymbol{\alpha}_{b,n+1}) : \frac{\partial \hat{\mathbf{n}}_{n+1}}{\partial \boldsymbol{\varepsilon}_{n+1}} + [\hat{\mathbf{n}}_{n+1} : (\boldsymbol{\alpha}_n - \boldsymbol{\alpha}_{b,n+1})] \frac{\partial \Delta\lambda}{\partial \boldsymbol{\varepsilon}_{n+1}} \\ &- (\boldsymbol{\alpha}_{n+1} - \boldsymbol{\alpha}_{b,n+1}) : \frac{\partial \boldsymbol{\alpha}_{b,n+1}}{\partial \boldsymbol{\varepsilon}_{n+1}} - (p_{n+1} - p^{\mathrm{e}}) R^2 \frac{\partial p_{n+1}}{\partial \boldsymbol{\varepsilon}_{n+1}} = 0 \end{aligned} \tag{109}$$

where it may be $p_{n+1} > 1$, in which case $\boldsymbol{\alpha}_{b,n+1} := \boldsymbol{\beta}_{b,n+1} = \boldsymbol{\sigma}_{0b,n+1}$ (the values for $p = 1$ before hardening). Note that as $\boldsymbol{\varepsilon}_{n+1}$ changes from iteration to iteration, also p_{n+1} does, and in consequence the term $\partial \boldsymbol{\alpha}_{b,n+1} / \partial \boldsymbol{\varepsilon}_{n+1}$ is generally not null:

$$\frac{\partial \boldsymbol{\alpha}_{b,n+1}}{\partial \boldsymbol{\varepsilon}_{n+1}} = \mathbf{b}_{n+1} \otimes \frac{\partial p_{n+1}}{\partial \boldsymbol{\varepsilon}_{n+1}} \tag{110}$$

As in the internal iterative process, there may be a derivative term not included in Equation (110) associated with the change in the tensors $\boldsymbol{\beta}_{b,n+1}, \boldsymbol{\sigma}_{0b,n+1}$ if there is a new unloading memory surface respect to the previous global iteration. As a result, there may be a loss of the second order convergence from the previous iteration to the actual one with similar consequences.

In Equations (109) and (110) $\partial p_{n+1} / \partial \boldsymbol{\varepsilon}_{n+1}$ is also not known and thus $\partial \Delta\lambda / \partial \boldsymbol{\varepsilon}_{n+1}$ may not be factored-out unless another equation is employed. This one is, as in the internal process, the difference between the constitutive equation for the internal plastic variables and the consistency one (supposed to be zero, or at least independent of $\boldsymbol{\varepsilon}_{n+1}$), Equation (72). Performing the $\boldsymbol{\varepsilon}_{n+1}$-derivative of this expression,

$$\frac{\partial \Delta\gamma^1}{\partial \boldsymbol{\varepsilon}_{n+1}} - \frac{\partial \Delta\gamma^2}{\partial \boldsymbol{\varepsilon}_{n+1}} = 0 \tag{111}$$

The first term is, from Equation (71):

$$\frac{\partial \Delta\gamma^1}{\partial \boldsymbol{\varepsilon}_{n+1}} = \hat{\mathbf{n}}_{n+1} - \frac{1}{2\mu} \frac{\partial \Delta\lambda}{\partial \boldsymbol{\varepsilon}_{n+1}} \tag{112}$$

whereas the second, as $\Delta\gamma^2 = \Delta\gamma_y + \Delta\gamma_b$, is

$$\frac{\partial \Delta\gamma^2}{\partial \boldsymbol{\varepsilon}_{n+1}} = \frac{\partial \Delta\gamma_y}{\partial \boldsymbol{\varepsilon}_{n+1}} + \frac{\partial \Delta\gamma_b}{\partial \boldsymbol{\varepsilon}_{n+1}} \tag{113}$$

where, since $\Delta\lambda = H_y \Delta\gamma_y$,

$$\frac{\partial \Delta\gamma_y}{\partial \boldsymbol{\varepsilon}_{n+1}} = \frac{1}{H_y} \frac{\partial \Delta\lambda}{\partial \boldsymbol{\varepsilon}_{n+1}} \tag{114}$$

The integral of the second term of (113), Equation (77), is evaluated numerically, so the integration procedure has to be included in order to obtain a consistently linearized algorithm. Taking the $\boldsymbol{\varepsilon}_{n+1}$-derivative of (81):

$$\frac{\partial \Delta\gamma_b}{\partial \boldsymbol{\varepsilon}_{n+1}} = \frac{\mathscr{H}(1-p_{n+1})}{p_{n+1}-p^s}\mathscr{S}_{2n}\{\Delta\gamma_p\}_{p^s}^{\bar{p}_{n+1}}\frac{\partial p_{n+1}}{\partial \boldsymbol{\varepsilon}_{n+1}} + \sum_{i=1}^{s,\bar{p}_{n+1}}\mathscr{S}_{2n}\left\{\frac{\partial \Delta\gamma_p(p)}{\partial \boldsymbol{\varepsilon}_{n+1}}\right\}_{p^{i-1}}^{p^s} \tag{115}$$

where for $0\leqslant q\leqslant 2n$ and $p = p^s + qh > p^s$

$$\frac{\partial \Delta\gamma_p(p)}{\partial \boldsymbol{\varepsilon}_{n+1}} = \frac{\partial}{\partial \boldsymbol{\varepsilon}_{n+1}}\left(\frac{1}{H_p}\langle \hat{\mathbf{n}}_{n+1} : \hat{\mathbf{m}}_{n+1}\rangle\langle \hat{\mathbf{n}}_{n+1} : \Delta\boldsymbol{\alpha}_p\rangle\right)\Big|_{p=p^s+qh} \tag{116a}$$

$$\begin{aligned} &= -\frac{1}{H_p}\frac{\partial H_p}{\partial p}\Big|_{p=p^s+qh}\frac{q}{2n}\frac{\partial p_{n+1}}{\partial \boldsymbol{\varepsilon}_{n+1}}\Delta\gamma_p \\ &\quad + \frac{\mathscr{H}(\hat{\mathbf{m}}_{n+1} : \Delta\boldsymbol{\alpha}_p)}{H_p}\langle \hat{\mathbf{m}}_{n+1} : \hat{\mathbf{n}}_{n+1}\rangle\left(\Delta\boldsymbol{\alpha}_p : \frac{\partial \hat{\mathbf{m}}_{n+1}}{\partial \boldsymbol{\varepsilon}_{n+1}} + \hat{\mathbf{m}}_{n+1} : \frac{\partial \Delta\boldsymbol{\alpha}_p}{\partial \boldsymbol{\varepsilon}_{n+1}}\right) \\ &\quad + \frac{\mathscr{H}(\hat{\mathbf{m}}_{n+1} : \hat{\mathbf{n}}_{n+1})}{H_p}\left(\hat{\mathbf{n}}_{n+1} : \frac{\partial \hat{\mathbf{m}}_{n+1}}{\partial \boldsymbol{\varepsilon}_{n+1}} + \hat{\mathbf{m}}_{n+1} : \frac{\partial \hat{\mathbf{n}}_{n+1}}{\partial \boldsymbol{\varepsilon}_{n+1}}\right) \end{aligned} \tag{116b}$$

and from (62)

$$\frac{\partial \Delta\boldsymbol{\alpha}_p(p = p^s + qh > p^s)}{\partial \boldsymbol{\varepsilon}_{n+1}} = \frac{\partial \boldsymbol{\alpha}_{n+1}}{\partial \boldsymbol{\varepsilon}_{n+1}} + (r - pR)\frac{\partial \hat{\mathbf{m}}_{n+1}}{\partial \boldsymbol{\varepsilon}_{n+1}} - \frac{qR}{2n}\mathbf{t}_{n+1}\otimes\frac{\partial p_{n+1}}{\partial \boldsymbol{\varepsilon}_{n+1}} \tag{117}$$

with $\mathbf{t}_{n+1}$ given by (98). As before, expression (116b) may be used for the case $p < p^s$ setting $\partial H_p/\partial p = 0$.

Note that (115) may be expressed as a function of only two unknown second-order tensors, $\partial\Delta\lambda/\partial\boldsymbol{\varepsilon}_{n+1}$ and $\partial p_{n+1}/\partial\boldsymbol{\varepsilon}_{n+1}$, since from (56)

$$\frac{\partial \hat{\mathbf{m}}_{n+1}}{\partial \boldsymbol{\varepsilon}_{n+1}} = \frac{1}{\|\mathbf{m}_{n+1}\|}\mathbb{P}_{\mathbf{m}} : \left[\frac{\partial \boldsymbol{\alpha}_{n+1}}{\partial \boldsymbol{\varepsilon}_{n+1}} - \mathbf{b}_{n+1}\otimes\frac{\partial p_{n+1}}{\partial \boldsymbol{\varepsilon}_{n+1}}\right] \tag{118}$$

where $\partial\boldsymbol{\alpha}_{n+1}/\partial\boldsymbol{\varepsilon}_{n+1}$ is given by (108) and the last term of this equation is explicitly known from (107).

In consequence, an equation in $\partial\Delta\lambda/\partial\boldsymbol{\varepsilon}_{n+1}$ and $\partial p_{n+1}/\partial\boldsymbol{\varepsilon}_{n+1}$ may be formed, which combined with (109) leads to a tensorial system of two equations and two unknowns. Factoring-out $\partial p_{n+1}/\partial\boldsymbol{\varepsilon}_{n+1}$ from (109), after some algebra leads to

$$\frac{\partial p_{n+1}}{\partial \boldsymbol{\varepsilon}_{n+1}} = \frac{b}{a}\frac{\partial \Delta\lambda}{\partial \boldsymbol{\varepsilon}_{n+1}} + \frac{\Delta\lambda}{a}(\boldsymbol{\alpha}_n - \boldsymbol{\alpha}_{b,n+1}) : \frac{\partial \hat{\mathbf{n}}_{n+1}}{\partial \boldsymbol{\varepsilon}_{n+1}} \tag{119}$$

with a and b given by (91) and (92), respectively.

Substituting (119) into (118), (117) and (116b), and inserting (108) into (118), this one into (117) and the result into (116b), the second-order tensor $\partial\Delta\gamma_b/\partial\boldsymbol{\varepsilon}_{n+1}$ is obtained, after some lengthy but straightforward algebra, as a function of $\partial\Delta\lambda/\partial\boldsymbol{\varepsilon}_{n+1}$. This tensor, altogether

with (114) and (112) may be substituted into (111) yielding

$$\frac{\partial \Delta\lambda}{\partial \boldsymbol{\varepsilon}_{n+1}} = 2\zeta \left[\hat{\mathbf{n}}_{n+1} + \boldsymbol{\psi} : \frac{\partial \hat{\mathbf{n}}_{n+1}}{\partial \boldsymbol{\varepsilon}_{n+1}} \right] \tag{120}$$

where

$$\frac{1}{2\zeta} := \frac{1}{2\mu} + \frac{1}{H_y} + \frac{b}{a}\phi + \sum_{i=1}^{s,\,\bar{p}_{n+1}} \mathscr{S}_{2n}\{\delta\phi_2\}_{p^{i-1}}^{p^i} \tag{121a}$$

$$\boldsymbol{\psi} := -\frac{\Delta\lambda}{a}(\boldsymbol{\alpha}_n - \boldsymbol{\alpha}_{b,n+1})\phi - \sum_{i=1}^{s,\,\bar{p}_{n+1}} \mathscr{S}_{2n}\{\delta\boldsymbol{\varphi}\}_{p^{i-1}}^{p^i} \tag{121b}$$

and

$$\delta := \mathscr{H}(\hat{\mathbf{m}}_{n+1} : \hat{\mathbf{n}}_{n+1})\mathscr{H}(\hat{\mathbf{m}}_{n+1} : \Delta\boldsymbol{\alpha}_p) \tag{122a}$$

$$\phi := \frac{\mathscr{H}(1 - p_{n+1})}{p_{n+1} - p^s} \mathscr{S}_{2n}\{\Delta\gamma_p\}_{p^s}^{\bar{p}_{n+1}} - \sum_{i=1}^{s,\,\bar{p}_{n+1}} \mathscr{S}_{2n}\{\delta\phi_1\}_{p^{i-1}}^{p^i} \tag{122b}$$

$$\begin{aligned}\phi_1 := {} & \frac{\Delta\gamma_p}{H_p}\frac{\partial H_p}{\partial p} q + \frac{(\hat{\mathbf{m}}_{n+1} : \Delta\boldsymbol{\alpha}_p)}{H_p \|\mathbf{m}_{n+1}\|} C_{nPb} \\ & + \frac{C_{mn}}{H_p \|\mathbf{m}_{n+1}\|} \mathbf{b}_{n+1} : \mathbb{P}_{\mathbf{m}} : \Delta\boldsymbol{\alpha}_p + \frac{RC_{mn}}{2n}\frac{qC_{mt}}{H_p}\end{aligned} \tag{122c}$$

$$\boldsymbol{\varphi} := \Delta\lambda\boldsymbol{\varphi}_2 + \frac{\hat{\mathbf{m}}_{n+1} : \Delta\boldsymbol{\alpha}_p}{H_p}\hat{\mathbf{m}}_{n+1} \tag{122d}$$

$$\boldsymbol{\varphi}_2 := \frac{(\hat{\mathbf{m}}_{n+1} : \Delta\boldsymbol{\alpha}_p)}{H_p \|\mathbf{m}_{n+1}\|}(\mathbb{P}_{\mathbf{m}} : \hat{\mathbf{n}}_{n+1}) + \frac{C_{mn}}{H_p \|\mathbf{m}_{n+1}\|}\mathbb{P}_{\mathbf{m}} : \Delta\boldsymbol{\alpha}_p + \frac{C_{mn}}{H_p}\hat{\mathbf{m}}_{n+1} \tag{122e}$$

$$\phi_2 := \hat{\mathbf{n}}_{n+1} : \boldsymbol{\varphi}_2 \tag{122f}$$

$$C_{mn} := \langle \hat{\mathbf{m}}_{n+1} : \hat{\mathbf{n}}_{n+1} \rangle \tag{122g}$$

$$C_{nPn} := \hat{\mathbf{n}}_{n+1} : \mathbb{P}_{\mathbf{m}} : \hat{\mathbf{n}}_{n+1} = 1 - (\hat{\mathbf{m}}_{n+1} : \hat{\mathbf{n}}_{n+1})^2 \tag{122h}$$

$$C_{nPb} := \hat{\mathbf{n}}_{n+1} : \mathbb{P}_{\mathbf{m}} : \mathbf{b}_{n+1} = \hat{\mathbf{n}}_{n+1} : \mathbf{b}_{n+1} - (\hat{\mathbf{n}}_{n+1} : \hat{\mathbf{m}}_{n+1})(\hat{\mathbf{m}}_{n+1} : \mathbf{b}_{n+1}) \tag{122i}$$

$$C_{mt} := \hat{\mathbf{m}}_{n+1} : \mathbf{t}_{n+1} \tag{122j}$$

Once (120) is known it may be substituted in (108) and the result, altogether with (107) into (106):

$$\frac{\partial \boldsymbol{\sigma}_{n+1}}{\partial \boldsymbol{\varepsilon}_{n+1}} = 2\zeta(\hat{\mathbf{n}}_{n+1} \otimes \hat{\mathbf{n}}_{n+1}) + [(r + \Delta\lambda)\mathbb{I} + 2\zeta\hat{\mathbf{n}}_{n+1} \otimes \boldsymbol{\psi}] : \frac{\partial \hat{\mathbf{n}}_{n+1}}{\partial \boldsymbol{\varepsilon}_{n+1}} \tag{123a}$$

$$= 2\zeta(\hat{\mathbf{n}}_{n+1}\otimes\hat{\mathbf{n}}_{n+1}) + \frac{2\mu(r+\Delta\lambda)}{\|\mathbf{n}^{\mathrm{tr}}_{n+1}\|}(\mathbb{I} - \hat{\mathbf{n}}_{n+1}\otimes\hat{\mathbf{n}}_{n+1})$$

$$+ \frac{4\zeta\mu}{\|\mathbf{n}^{\mathrm{tr}}_{n+1}\|}\hat{\mathbf{n}}_{n+1}\otimes[\boldsymbol{\psi} - (\boldsymbol{\psi}:\hat{\mathbf{n}}_{n+1})\hat{\mathbf{n}}_{n+1}] \tag{123b}$$

$$= 2\mu\bar{\zeta}_{nn}\hat{\mathbf{n}}_{n+1}\otimes\hat{\mathbf{n}}_{n+1} + 2\mu\bar{\zeta}_{n\psi}\hat{\mathbf{n}}_{n+1}\otimes\boldsymbol{\psi} + \frac{2\mu(r+\Delta\lambda)}{\|\mathbf{n}^{\mathrm{tr}}_{n+1}\|} \tag{123c}$$

with

$$\bar{\zeta}_{n\psi} = \frac{2\zeta}{\|\mathbf{n}^{\mathrm{tr}}_{n+1}\|} \tag{124a}$$

$$\bar{\zeta}_{nn} = \frac{2\zeta}{2\mu} - \frac{r+\Delta\lambda}{\|\mathbf{n}^{\mathrm{tr}}_{n+1}\|} - \bar{\zeta}_{n\psi}(\boldsymbol{\psi}:\hat{\mathbf{n}}_{n+1}) \tag{124b}$$

Finally, (123c) may be introduced in (101) to obtain the algorithmic elastoplastic tangent in closed form

$$\mathbb{C}^{\mathrm{ep}} = \left(K - \frac{2\mu(r+\Delta\lambda)}{3\|\mathbf{n}^{\mathrm{tr}}_{n+1}\|}\right)\mathbf{I}\otimes\mathbf{I} + \frac{2\mu(r+\Delta\lambda)}{\|\mathbf{n}^{\mathrm{tr}}_{n+1}\|}\mathbb{I} + 2\mu\bar{\zeta}_{nn}\hat{\mathbf{n}}_{n+1}\otimes\hat{\mathbf{n}}_{n+1} + 2\mu\bar{\zeta}_{n\psi}\hat{\mathbf{n}}_{n+1}\otimes\boldsymbol{\psi} \tag{125}$$

which is a tensor with minor symmetries and with lack of the major one in the general case of non-proportional loading due to the last term.

6. IMPLEMENTATION

Boxes I–VII sketch the implementation of the algorithm in a typical finite elements code. In this implementation, three issues are relevant.

6.1. Computationally efficient expressions

The first one is the computation of the numerical integrations through the composite Simpson operator. This may be an expensive task, since it will be performed in every internal iteration (once for every trial p^i_{n+1}). In consequence it should be programmed in an efficient way. To do so, the linear property of the operator, given by (80), may be employed. Aside, as it will be seen, the consistency parameter, the internal tangent and the global tangent use similar expressions inside the Simpson operator, so it is usually efficient to compute all the terms involved at the same time.

After grouping terms in Equations (90)–(99) one can obtain for (88) the following expression:

$$\frac{\mathrm{d}\mathit{Error}}{\mathrm{d}p_{n+1}} = -\frac{1}{2\zeta}\frac{\mathrm{d}\lambda}{\mathrm{d}p_{n+1}}$$

Box I. Stress-point algorithm.

Input variables: $\boldsymbol{\sigma}_n^{\mathrm{f}}, R, \Delta\boldsymbol{\varepsilon}^{\mathrm{f}}, \mu, K, \{\boldsymbol{\alpha}^i, p^i, i=0,\ldots,u+2\}$, where $\boldsymbol{\alpha}^0=\boldsymbol{\beta}_{b,n}$ and where $\boldsymbol{\alpha}^{u+1}=\boldsymbol{\alpha}_{b,n}$, $p^{u+1}=p_n$, $\boldsymbol{\alpha}^{u+2}=\boldsymbol{\alpha}$, $p^{u+2}=p^e$

Start: $\boldsymbol{\sigma}_{n+1}^{\mathrm{tr}}=\boldsymbol{\sigma}_n+2\mu\Delta\boldsymbol{\varepsilon}$; $\mathbf{n}_{n+1}^{\mathrm{tr}}=\boldsymbol{\sigma}_{n+1}^{\mathrm{tr}}-\boldsymbol{\alpha}_n$; $n_{n+1}^{\mathrm{tr}}=\|\mathbf{n}_{n+1}^{\mathrm{tr}}\|$; $\hat{\mathbf{n}}_{n+1}\leftarrow\mathbf{n}_{n+1}^{\mathrm{tr}}/n_{n+1}^{\mathrm{tr}}$

Elastic step: if $n_{n+1}^{\mathrm{tr}}\leqslant r$, $\boldsymbol{\sigma}_{n+1}\leftarrow\boldsymbol{\sigma}_n+2\mu\Delta\boldsymbol{\varepsilon}$; $\mathbb{C}_{n+1}^{\mathrm{ep}}\leftarrow K\mathbf{I}\otimes\mathbf{I}+2\mu(\mathbb{I}-\frac{1}{3}\mathbf{I}\otimes\mathbf{I})$; end process.

Plastic step: $\mathbf{b}_n=\boldsymbol{\beta}_{bn}-\boldsymbol{\sigma}_{0bn}$; $\boldsymbol{\alpha}_{b,n}=\boldsymbol{\sigma}_{0bn}+p_n\mathbf{b}_n$;

$\mathbf{m}_n=\boldsymbol{\alpha}_n-\boldsymbol{\alpha}_{b,n}$; $m_n=\|\mathbf{m}_n\|$; $\hat{\mathbf{m}}_n=\mathbf{m}_n/m_n$; $C_{mn}^n=\hat{\mathbf{n}}_{n+1}:\hat{\mathbf{m}}_n$

Need-for-new-homology: IF $C_{mn}^n<0$ THEN
- Save values: process Box II, task '*save*'
- Update: $p_n\leftarrow p^e$; $\boldsymbol{\sigma}_{0bn}\leftarrow\boldsymbol{\alpha}_n+r\hat{\mathbf{m}}_n$; $\boldsymbol{\beta}_{bn}\leftarrow\boldsymbol{\alpha}_n+(r-R)\hat{\mathbf{m}}_n$
- GOTO Plastic step

Iterative process: Initial guess $p_{n+1}\leftarrow p_n+\bar{\delta}$ with $\bar{\delta}\rightarrow 0$

Iteration: process Box III, computation of $\boldsymbol{\sigma}_{0b,n+1}, \boldsymbol{\beta}_{b,n+1}$ (for p_{n+1})

$\mathbf{b}_{n+1}=\boldsymbol{\sigma}_{0b,n+1}-\boldsymbol{\beta}_{b,n+1}$; $\boldsymbol{\alpha}_{b,n+1}=\boldsymbol{\sigma}_{0b}+p_{n+1}\mathbf{b}_{n+1}$;

$\bar{b}=\hat{\mathbf{n}}_{n+1}:(\boldsymbol{\alpha}_n-\boldsymbol{\alpha}_{b,n+1})$; $\bar{c}=\|\boldsymbol{\alpha}_n-\boldsymbol{\alpha}_{b,n+1}\|^2-(p_{n+1}-p^e)^2R^2$; $\Delta\lambda=-\bar{b}+\sqrt{\bar{b}^2-\bar{c}}$

$\boldsymbol{\alpha}_{n+1}=\boldsymbol{\alpha}_n+\Delta\lambda\hat{\mathbf{n}}_{n+1}$; $\mathbf{m}_{n+1}=\boldsymbol{\alpha}_{n+1}-\boldsymbol{\alpha}_{b,n+1}$; $m_{n+1}=\|\mathbf{m}_{n+1}\|$; $\hat{\mathbf{m}}_{n+1}=\mathbf{m}_{n+1}/m_{n+1}$

Compute coefficients independent of p:

$C_{mn}=\hat{\mathbf{m}}_{n+1}:\hat{\mathbf{n}}_{n+1}$; $C_{nPn}=1-C_{mn}^2$;

$b=\Delta\lambda+\bar{b}$; $a=(p_{n+1}-p^e)R^2+(\mathbf{m}_{n+1}:\mathbf{b}_{n+1})$; $\mathrm{d}\lambda=a/b$; $\Delta\hat{\mathbf{m}}=\hat{\mathbf{m}}_{n+1}-\hat{\mathbf{m}}_n$;

Process Box V: obtain $[C_{s1}, C_{s2}, C_{s3}, \mathbf{a}_b]$; $\Delta\gamma_b=C_{mn}\hat{\mathbf{m}}_{n+1}:\mathbf{a}_b$

$$Error=\frac{n_{n+1}^{\mathrm{tr}}-r}{2\mu}-\left(\frac{1}{2\mu}+\frac{1}{Hy}\right)\Delta\lambda-\Delta\gamma_b;$$

$(2\varsigma)^{-1}=$ see Equation (126)

IF $2\mu*Error<tolerance*R$ process Box VII (final update and computation of $\mathbb{C}_{n+1}^{\mathrm{ep}}$)

Tangent of the interior iterative process: $\mathrm{d}Error=-(2\varsigma)^{-1}\,\mathrm{d}\lambda$

Update: $p_{n+1}\leftarrow p_{n+1}-Error/\mathrm{d}Error$

where $\mathrm{d}\lambda/\mathrm{d}p_{n+1}=a/b$ with a,b given by (91) and (92). The factor $(2\zeta)^{-1}$ may be written as

$$\frac{1}{2\zeta}=\frac{1}{2\mu}+\frac{1}{H_y}+C_{nPn}\mathbf{m}_{n+1}:\mathbf{a}_b+C_{mn}^2C_{s1}+\frac{C_{mn}}{\|\mathbf{m}_{n+1}\|}[\mathbf{a}_p:\hat{\mathbf{n}}_{n+1}-C_{mn}(\mathbf{a}_p:\hat{\mathbf{m}}_{n+1})]+\phi_b\frac{b}{a} \tag{126}$$

with

$$\phi_b=\frac{\mathscr{H}(1-p_{n+1})}{p_{n+1}-p^s}\Delta\gamma_b-\frac{C_{s2}}{2n}-\frac{C_{nPn}}{\|\mathbf{m}_{n+1}\|}(\hat{\mathbf{m}}_{n+1}:\mathbf{a}_b)-\frac{RC_{mn}}{2n}C_{s3}$$
$$-\frac{C_{mn}}{\|\mathbf{m}_{n+1}\|}[\mathbf{a}_b:\mathbf{b}_{n+1}-(\mathbf{a}_b:\hat{\mathbf{m}}_{n+1})(\hat{\mathbf{m}}_{n+1}:\mathbf{b}_{n+1})] \tag{127}$$

Box II. Storage handler routine.

If task = '*remove*' then
  For $i=u$ to $i=0$ (step -1)
    If $p^i >= p$ exit loop setting $u=i$
  end loop
  update: $\boldsymbol{\alpha}^{u+1} \leftarrow \boldsymbol{\sigma}_0 + \min(p,1)(\boldsymbol{\beta}-\boldsymbol{\sigma}_0)$; $p^i \leftarrow \min(p,1)$; $\boldsymbol{\alpha}^{u+2} \leftarrow \boldsymbol{\alpha}$; $p^{u+2} \leftarrow p^e$,
If task = '*save*' (new homology)
  If $u=L$
    Compute $i^* = \arg\{\min(d^i = \sqrt{(p^{i-1}-p^i)^2 + (p^{i-2}-p^i)^2}; \quad i=1,\ldots,u-1)\}$
    Update $u \leftarrow u-1$ and eliminate i^*: $p^i \leftarrow p^{i+1}$; $\boldsymbol{\alpha}^i \leftarrow \boldsymbol{\alpha}^{i+1}$ for all $i=i^*,\ldots,u$
  end if
  New memory surface is the yield surface: $u \leftarrow u+1$, $p^u \leftarrow p^e$, $\boldsymbol{\alpha}^u \leftarrow \boldsymbol{\alpha}$

Box III. Computation of $\boldsymbol{\beta}_p$ and $\boldsymbol{\sigma}_{0p}$ for a given p.

if $p \geqslant (p^0 = 1)$ then $\boldsymbol{\beta}_p = \boldsymbol{\sigma}_{0p} = \boldsymbol{\alpha}^0$;
else,
  Locate i such that $p^i > p \geqslant p^{i+1}$

$$\boldsymbol{\sigma}_{0p,n} = \frac{p^{i+1}}{p^{i+1}-p^i}\boldsymbol{\alpha}^i - \frac{p^i}{p^{i+1}-p^i}\boldsymbol{\alpha}^{i+1},$$

$$\boldsymbol{\beta}_{p,n} = \frac{p^{i+1}-1}{p^{i+1}-p^i}\boldsymbol{\alpha}^i - \frac{p^i-1}{p^{i+1}-p^i}\boldsymbol{\alpha}^{i+1}$$

where

$$C_{s1} := \sum_{i=1}^{s,\bar{p}_{n+1}} \mathscr{S}_{2n}\left\{\frac{1}{H_p}\right\}_{p^{i-1}}^{p^i} \tag{128}$$

$$C_{s2} := \mathscr{H}(1-p_{n+1})C_{mn}\mathscr{S}_{2n}\left\{\frac{q}{H_p}\frac{\partial H_p}{\partial p}\bigg|_{p=p^e+qh}\left\langle \hat{\mathbf{m}}_{n+1} : \frac{\Delta\boldsymbol{\alpha}_p}{H_p}\right\rangle\right\}_{p^s}^{\bar{p}_{n+1}} \tag{129}$$

$$C_{s3} := \mathscr{S}_{2n}\left\{\frac{q}{H_p}C_{mt}\right\}_{p^s}^{\bar{p}_{n+1}} \tag{130}$$

$$\mathbf{a}_b := \sum_{i=1}^{s,\hat{p}_{n+1}} \mathscr{S}_{2n}\left\{\frac{\Delta\boldsymbol{\alpha}_p}{H_p}\right\}_{p^{i-1}}^{p^i} \tag{131}$$

Box IV. Numerical integration procedure.

Locate surfaces:

$s \leftarrow 0$

For $i = u$ to $i = 1$

If $p^i < p_{n+1}$ then $s \leftarrow s + 1$ (increments the number-of-crossing-surfaces index)

End

$[C_{s1}, \mathbf{a}_b] \leftarrow [0, \ldots, \mathbf{0}]$, $p^{(i-1)} \leftarrow p^e$, where the superindex $(i-1)$ is just a label, not a surface index

Option: Integrate always from p^e to p_n

$h \leftarrow \dfrac{p_n - p^e}{2n}$,

Process Box V for $p^{(i-1)} \leftarrow p^e$ and $p^{(i)} \leftarrow p_n$, obtaining $\mathscr{S}_{2n}\{[C_{s1\,p}, \mathbf{a}_p]\}_{p^{(i-1)}}^{p^{(i)}}$

$[C_{s1}, \mathbf{a}_b] \leftarrow [C_{s1}, \mathbf{a}_b] + \mathscr{S}_{2n}\{[C_{s1\,p}, \mathbf{a}_p]\}_{p^{(i-1)}}^{p^{(i)}}$

$p^{(i-1)} \leftarrow p_n$

Any option, integrate between crossed surfaces: For $j = 1$ to s

$p^{(i)} \leftarrow p^{u+1-i}$; $\quad h \leftarrow \dfrac{p^{(i)} - p^{(i-1)}}{2n}$;

Process Box V for the given $p^{(i-1)}$, $p^{(i)}$ and add results

$[C_{s1}, \mathbf{a}_b] \leftarrow [C_{s1}, \mathbf{a}_b] + \mathscr{S}_{2n}\{[C_{s1\,p}, \mathbf{a}_p]\}_{p^{(i-1)}}^{p^{(i)}}$

$p^{(i-1)} \leftarrow p^{(i)}$

Final integration:

$p^{(i)} \leftarrow \bar{p}_{n+1}$; $\quad h \leftarrow \dfrac{p^{(i)} - p^{(i-1)}}{2n}$;

Process Box V for the given $p^{(i-1)}$, $p^{(i)}$ and add results

$[C_{s1}, C_{s2}, C_{s3}, \mathbf{a}_b] \leftarrow [C_{s1}, 0, 0, \mathbf{a}_b] + \mathscr{S}_{2n}\{[C_{s1p}, C_{s2p}, C_{s3p}, \mathbf{a}_p]\}_{p^{(i-1)}}^{p^{(i)}}$

$C_{s2} \leftarrow C_{s2}\mathscr{H}(1 - p_{n+1})C_{mn}$

are the only terms that need to be integrated numerically, rendering the integration procedure a not-too-expensive task. Note that $\Delta\gamma_b := C_{mn}\hat{\mathbf{m}}_{n+1} : \mathbf{a}_b$ and that C_{s2} and C_{s3} are integrated only from p^s to $\bar{p}_{n+1}$ whereas C_{s1} and $\mathbf{a}_b$ from p^e to $\bar{p}_{n+1}$.

Similarly, to compute a more efficient version of Equation (123c), $\boldsymbol{\psi}$ may be written as

$$\boldsymbol{\psi} = -\phi_b \frac{\Delta\lambda}{a}(\boldsymbol{\alpha}_n - \boldsymbol{\alpha}_{b,n+1}) - \frac{\Delta\lambda}{\|\mathbf{m}_{n+1}\|}(\hat{\mathbf{n}}_{n+1} - C_{mn}\hat{\mathbf{m}}_{n+1})(\hat{\mathbf{m}}_{n+1} : \mathbf{a}_p)$$
$$-(\hat{\mathbf{m}}_{n+1} : \mathbf{a}_b)\hat{\mathbf{m}}_{n+1} - \Delta\lambda C_{mn}C_{s1}\hat{\mathbf{m}}_{n+1} - C_{mn}\frac{\Delta\lambda}{\|\mathbf{m}_{n+1}\|}[\mathbf{a}_p - (\mathbf{a}_p : \hat{\mathbf{m}}_{n+1})\hat{\mathbf{m}}_{n+1}] \quad (132)$$

whose terms do not need any further integration.

Box V. Composite Simpson operator $\mathscr{S}_{2n}\{\cdot\}_{p^{(i-1)}}^{p^{(i)}}$.

Initialize: $\mathscr{S}_{2n}\{\cdot\}_{p^{(i-1)}}^{p^{(i)}} = (\cdot)_{p^{(i-1)}}$;
Do $\eta = 1$ to $n-1$
  $q \leftarrow 2\eta - 1$; $\mathscr{S}_{2n}\{\cdot\}_{p^{(i-1)}}^{p^{(i)}} \leftarrow \mathscr{S}_{2n}\{\cdot\}_{p^{(i-1)}}^{p^{(i)}} + 4(\cdot)_{p=p^{(i-1)}+qh}$
  $q \leftarrow 2\eta$; $\mathscr{S}_{2n}\{\cdot\}_{p^{(i-1)}}^{p^{(i)}} \leftarrow \mathscr{S}_{2n}\{\cdot\}_{p^{(i-1)}}^{p^{(i)}} + 2(\cdot)_{p=p^{(i-1)}+qh}$
End do
$q \leftarrow 2n-1$; $\mathscr{S}_{2n}\{\cdot\}_{p^{(i-1)}}^{p^{(i)}} \leftarrow \mathscr{S}_{2n}\{\cdot\}_{p^{(i-1)}}^{p^{(i)}} + 4(\cdot)_{p=p^{(i-1)}+qh}$
$\mathscr{S}_{2n}\{\cdot\}_{p^{(i-1)}}^{p^{(i)}} \leftarrow \dfrac{h}{3}[\mathscr{S}_{2n}\{\cdot\}_{p^{(i-1)}}^{p^{(i)}} + (\cdot)_{p=p^{(i)}}]$

Box VI. Computation of the terms inside the composite Simpson operator $[C_{s1p}, C_{s2p}, C_{s3p}, \mathbf{a}_p]$ such that $[C_{s1}, C_{s2}, C_{s3}, \mathbf{a}_b] \leftarrow \mathscr{S}_{2n}\{[C_{s1p}, C_{s2p}, C_{s3p}, \mathbf{a}_p]\}_{p^{(i-1)}}^{p^{(i)}}$.

Initialize: $p = p^{(i-1)} + qh$
Compute inverse of hardening function $C_{s1p} = H_p^{-1}(p)$ (Function given by the user)
Compute $\Delta\boldsymbol{\alpha}_p$
  If $p \leqslant p_n$ then
    $\Delta\boldsymbol{\alpha}_p = \Delta\lambda\hat{\mathbf{n}}_{n+1} - qhR\,\Delta\hat{\mathbf{m}}$;
  else,
    Process Box III for p to obtain $\boldsymbol{\beta}_{p,n}$ and $\boldsymbol{\sigma}_{0p,n}$. Define $\mathbf{b}_{pn} = \boldsymbol{\beta}_{p,n} - \boldsymbol{\sigma}_{0p,n}$
    $\Delta\boldsymbol{\alpha}_p = \boldsymbol{\alpha}_{n+1} - \boldsymbol{\sigma}_{0p,n} - qhR\,\hat{\mathbf{m}}_{n+1} - p\mathbf{b}_{pn}$
$\mathbf{a}_p = C_{s1p}\Delta\boldsymbol{\alpha}_p$
If *option* = 'free end': Compute C_{s2p}, C_{s3p}
  Compute $\left.\dfrac{\mathrm{d}H_p}{\mathrm{d}p}\right|_p$ (Function given by the user)
  $C_{s2p} = (qC_{s1p})\left.\dfrac{\mathrm{d}H_p}{\mathrm{d}p}\right|_p \langle\hat{\mathbf{m}}_{n+1} : \mathbf{a}_p\rangle$
  $C_{s3p} = (qC_{s1p})(1 + \hat{\mathbf{m}}_{n+1} : \mathbf{b}_{pn}/R)$

6.2. *Handling of storage memory*

The second one is the storage strategy for the memory tensors and radii of the 'unloading' surfaces $\{\boldsymbol{\alpha}^i, p^i\}$. In this model, since any 'unloading' (new homology) event generates a new memory surface, the amount of surfaces could become very large for some loading cases. Therefore, it is necessary to prescribe a maximum number of surfaces L. Once the limit is reached, it is necessary to search for the less significative events. These are the ones

Box VII. Final update and computation of the algorithmic elastoplastic tangent $\mathbb{C}^{\text{ep}}$.

Final update of the stress tensor: $\boldsymbol{\sigma}^{\text{f}}_{n+1} = \boldsymbol{\alpha}_{n+1} + r\hat{\mathbf{n}}_{n+1} + K\,\text{tr}(\boldsymbol{\varepsilon}^{\text{f}}_{n+1})\mathbf{I}$
Computation of the tangents:
If *convergence phase* then
  Return elastic tangent $\mathbb{C}^{\text{ep}}_{n+1} \leftarrow K\mathbf{I}\otimes\mathbf{I} + 2\mu(\mathbb{I} - \frac{1}{3}\mathbf{I}\otimes\mathbf{I})$
  If $p_{n+1} > 1$ update position of the bounding surface: $\boldsymbol{\beta}_{n+1} = \boldsymbol{\alpha}_{n+1} + (p^e - 1)R\hat{\mathbf{m}}_{n+1}$
  Process Box II to '*remove*' $p^i < p_{n+1}$ surfaces
  and account for hypoplasticity, Equations (134) and (135)
else
  $\boldsymbol{\psi} =$ see Equation (132)
  $\bar{\zeta}_{n\psi} = \dfrac{2\zeta}{n^{\text{tr}}_{n+1}}; \quad \tilde{a} = \dfrac{2\mu(r+\Delta\lambda)}{n^{\text{tr}}_{n+1}}$
  $(2\mu\bar{\zeta}_{nn}) = 2\zeta - \tilde{a} - 2\mu\bar{\zeta}_{n\psi}(\hat{\mathbf{n}}_{n+1} : \boldsymbol{\psi})$
  $\mathbb{C}^{\text{ep}}_{n+1} = \left(K - \dfrac{\tilde{a}}{3}\right)\mathbf{I}\otimes\mathbf{I} + \tilde{a}\mathbb{I} + (2\mu\bar{\zeta}_{nn})\hat{\mathbf{n}}_{n+1}\otimes\hat{\mathbf{n}}_{n+1} + 2\mu\bar{\zeta}_{n\psi}\hat{\mathbf{n}}_{n+1}\otimes\boldsymbol{\psi}$

that are close to another one in the stress space. Therefore, we can eliminate that event i with the minimum absolute distance to the adjacent ones in the sense

$$d_i = \sqrt{(p^i - p^{i-1})^2 + (p^i - p^{i+1})^2} \tag{133}$$

where $1 \leqslant i \leqslant u$, ($u$ is the last memory surface for the given stress integration point) and $p^{u+1} = p_n$, $p^0 = 1$. This strategy is implemented in Box II, and allows that with a very small number of surfaces a good cyclic description is obtained.

6.3. *Lack of convexity of the error function*

The function $error^i$ is not convex in the whole domain where it is well posed, although it has only one root and therefore, since it is a scalar equation a solution is guaranteed to be found if a proper method is selected. The Newton–Raphson algorithm may diverge if the guess is not good enough. Alternatives are a line-search or the simplest bisection method if divergence is detected. Once a good approximation is known, we may return to the Newton method to obtain the solution to the desired tolerance in few iterations.

7. STRESS-POINT EXAMPLES

Figure 4 shows the uniaxial behaviour of the model. Material data for the example (typical for a soil) are summarized in Table I. As expected, the Masing rules are preserved; i.e. loops are closed, the unloading curve has an homological ratio of two with the virgin one and this last one is recovered once the previous level of stresses is recovered. The advantage over the

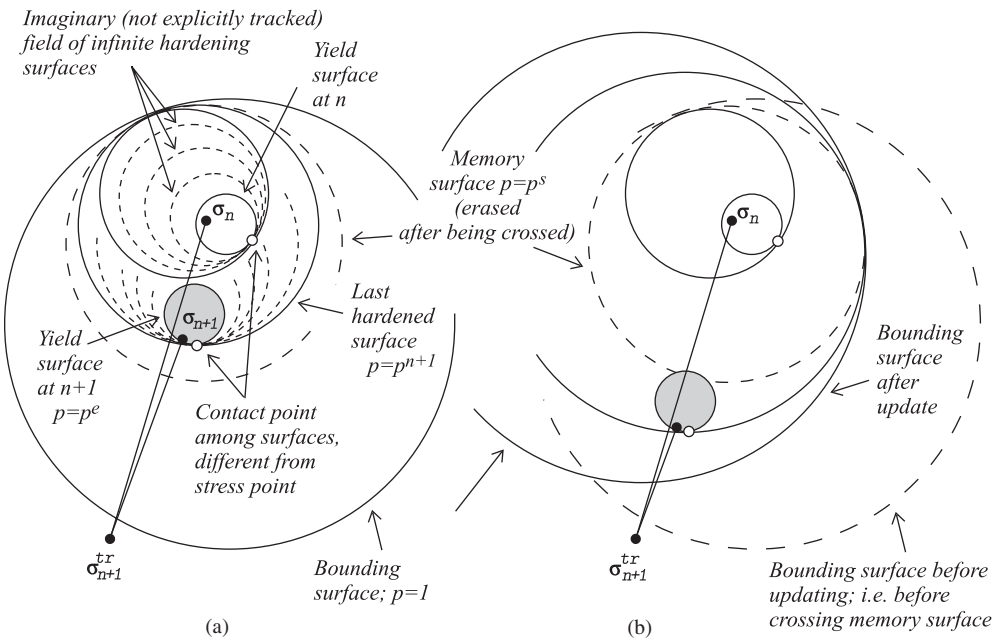

Figure 4. Integration procedure: (a) if the yield surface does not pass over a memory surface; and (b) if the yield surface passes over a memory surface.

Table I. Material data for the stress-point examples (units: adimensional or kPa where applicable).

Virtual bounding surface*	Multilayer w/Prager's rule†	Multilayer w/Mróz's rule‡
$h = 1.48 \times 10^4$	$r_1 = 1.71,\ H_1 = 81.5 \times 10^5$	$r_1 = 14.4,\ H_1 = 3.95 \times 10^5$
$m = 1.4$	$r_2 = 5.88,\ H_2 = 9.20 \times 10^5$	$r_2 = 24.1,\ H_2 = 6.46 \times 10^5$
$H_y \to \infty$	$r_3 = 14.5,\ H_3 = 3.41 \times 10^5$	$r_3 = 35.9,\ H_3 = 2.70 \times 10^5$
$H_0 = 4.4 \times 10^5$	$r_4 = 35.9,\ H_4 = 1.46 \times 10^5$	$r_4 = 49.9,\ H_4 = 2.21 \times 10^5$
$R = 176$	$r_5 = 66.4,\ H_5 = 2.05 \times 10^5$	$r_5 = 66.3,\ H_5 = 17.4 \times 10^5$
	$r_6 = 154,\ H_6 = 3.21 \times 10^5$	$r_6 = 106,\ H_6 = 2.48 \times 10^5$

Young's modulus for all the models: $E = 3.7 \times 10^5$
Poisson's ratio for all the models: $\nu = 0.45$

*Obtained from the prescribed points (shear moduli ratio, engrg. shear strain)
$\{(\mu/\mu_{\max} = 0.81, \gamma = 0.01\%), (0.375, 0.1\%), (0.1, 1\%)\}$.
†Obtained from the prescribed points:
$\{(0.97, 0.001\%), (0.95, 0.0035\%), (0.81, 0.01\%), (0.58, 0.035\%), (0.375, 0.1\%), (0.25, 0.35\%)\}$.
‡Obtained from the prescribed points:
$\{(0.81, 0.01\%), (0.68, 0.02\%), (0.58, 0.035\%), (0.47, 0.06\%), (0.375, 0.1\%), (0.3, 0.2\%)\}$.

multilayer simulation (also shown in the figure) is that the curve is smooth and no additional errors are introduced during unloading events, since they are consistently located. Furthermore, the memory surfaces will always be at optimum locations and have optimum radii since they are generated at the 'unloading' events.

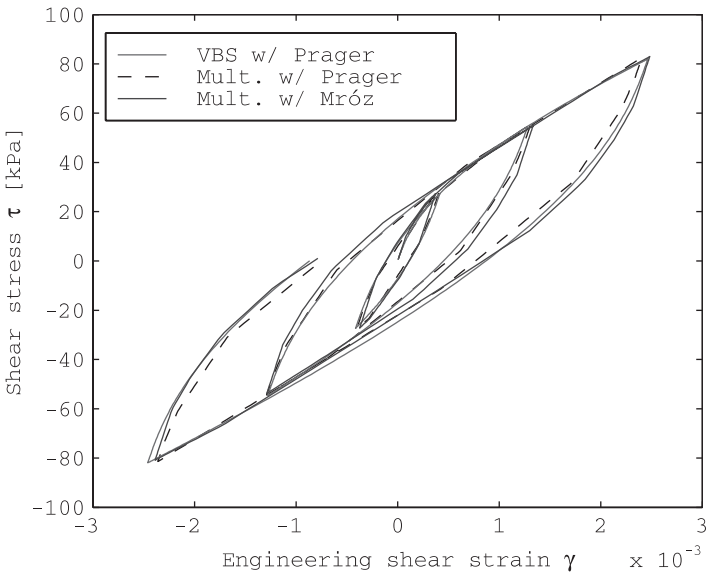

Figure 5. Typical uniaxial stress–strain loops using multilayer plasticity and virtual bounding surface plasticity (VBS).

The right part of Figure 6 shows the multiaxial coupling of the model for the loading path shown in its left part. In the same figure they are represented the paths obtained with multilayer plasticity using both the Prager and the Mróz rules and the model of Reference [17]. The implicit formulation of the multilayer model using the Mróz curve necessitates a maximum ratio of two between consecutive surfaces, so the properties were modified to fulfill this requirement. These data are shown also in Table I.

One could expect the model presented here to behave closer to the multilayer plasticity one using Prager's rule, since both models have distinct similarities. Nonetheless, note that the structure of the hardening is closer to the multilayer model using Mróz's rule, since all the hardening surfaces contact at the same point (although now different from the actual stress).

On the other hand, the behaviour exhibited by the multilayer model using the Prager rule is desired for some materials like soils and it is sometimes termed as hypoplasticity in the context of bounding surface plasticity [14, 19, 20]. The next paragraphs elaborate this point, since this type of behaviour has been necessary to obtain acceptable results for the Lotung problem.

8. 'HYPOPLASTIC' BEHAVIOUR

In this model it is possible to control that behaviour independently of the rest of the model. This is due to the fact that this type of behaviour is given by the value of the product $(\hat{\mathbf{m}}:\hat{\mathbf{n}})$, and the translation direction of the surfaces does not have to be necessarily $\hat{\mathbf{m}}$. Any other direction combination of $\hat{\mathbf{n}}$ and $\hat{\mathbf{m}}$ may be utilized if it is properly accounted for in Equation (33) and so on. Nonetheless, given the independence of the stress point from the

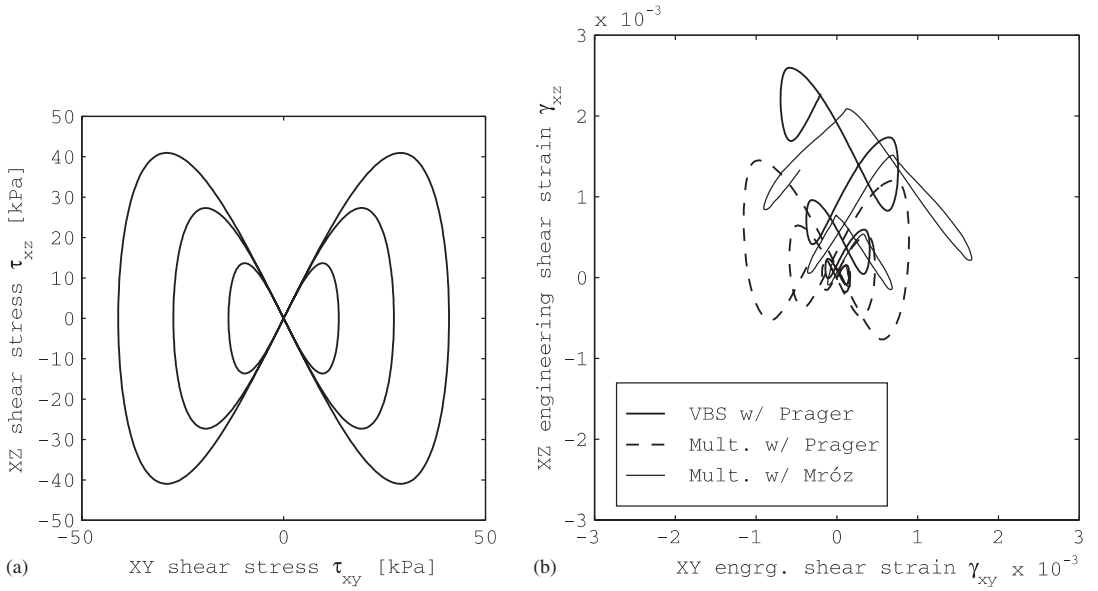

Figure 6. Multiaxial coupling with the different models: (a) imposed stress path; and (b) obtained strain paths.

contact point, it is possible to use a simpler *a posteriori*, explicit approach. Since with the hardening the contact point moves towards the stress point, consider an acceleration of this process governed by the following direction

$$\hat{\mathbf{y}} := \mathbf{y}/\|\mathbf{y}\| \quad \text{with } \mathbf{y} := \hat{\mathbf{n}} + (\hat{\mathbf{m}} - \hat{\mathbf{n}}) \exp\left[-\left(\frac{\Delta\lambda}{R} \right)^{C} \Big/ \tau \right] \tag{134}$$

where τ is a material relaxation parameter and C is a material constant. In the convergence phase, the position of the memory surfaces may be corrected to the contact direction with the following simple update formula:

$$\boldsymbol{\alpha}^i = \boldsymbol{\alpha} + (p^e - p^i) R \hat{\mathbf{y}} \tag{135}$$

Note that the stresses and strains are not modified and the consistency of the model is kept, so the properties of the implicit algorithm are not altered. Figure 7 shows the influence of τ on the strain path of the previous section for $C = 1$. Material data are still the same. Basically, this modification changes the effective hardening modulus in multiaxial loading. Other expressions distinct from Equation (134) are also possible, but unexplored as of yet in this work.

9. APPLICATION TO SOIL DYNAMICS

The model has been applied to soil dynamics, which presents a severe test for models for cyclic behaviour. Note that, since the model is deviatoric, no pore pressure build-up can be

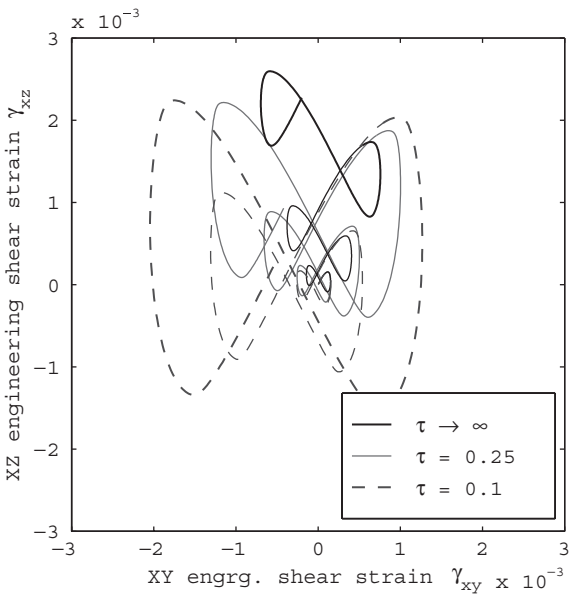

Figure 7. Influence of the parameter τ on the strain paths of the multiaxial simulation.

accounted for. The Electric Power Research Institute (EPRI) and the Taiwan Power Company (TPC) instrumented the Lotung large-scale seismic test site (LSST) in Taiwan and recorded several earthquakes. The earthquake is the event known as LSST07, that took place on 20 May 1986 (see References [25–27] for the background). Instrumentation arrays have been installed at different depths and locations to capture the free-field response and the SSI effects. In this example, we use the DHB47 (free-field motion at 47 m depth) north–south (N–S) and east–west (E–W) recordings as input motions and obtain predictions at the ground surface, which is then compared to the ground-surface accelerometer at the site. The type of finite elements and discretization are the same as those used in References [8, 21], where the same event is analysed using different formulations of the constitutive model. The shear moduli profile and shear moduli degradation curves are also the same as those employed in the cited references and reported in Reference [26]. The parameters h and m of the hardening function have been obtained from the shear moduli reduction curve solving a system of two non-linear equations in which the known data are two points of that curve. The process has been already reported for similar models (see for example References [8, 21, 28]). The value of the radius of the bounding surface has been estimated also from a third point on the shear moduli reduction curve. The hardening H_0 associated to the bounding is estimated from the secant shear modulus at that third point, as also reported on those references. The only parameter distinct from those reported in the literature is the τ parameter. A value of τ approaching infinity which corresponds to the basic model did not give acceptable results. A similar inaccuracy happened with the multilayer model using Mróz's translation rule (see Reference [8]); in contrast with what happened with the multilayer plasticity using Prager's rule. A value of $\tau = 0.25$ give the results shown in Figures 8–10. An explanation may be obtained observing Figure 7. Note that for this value of τ, both the multilayer model using Prager's rule and the model presented

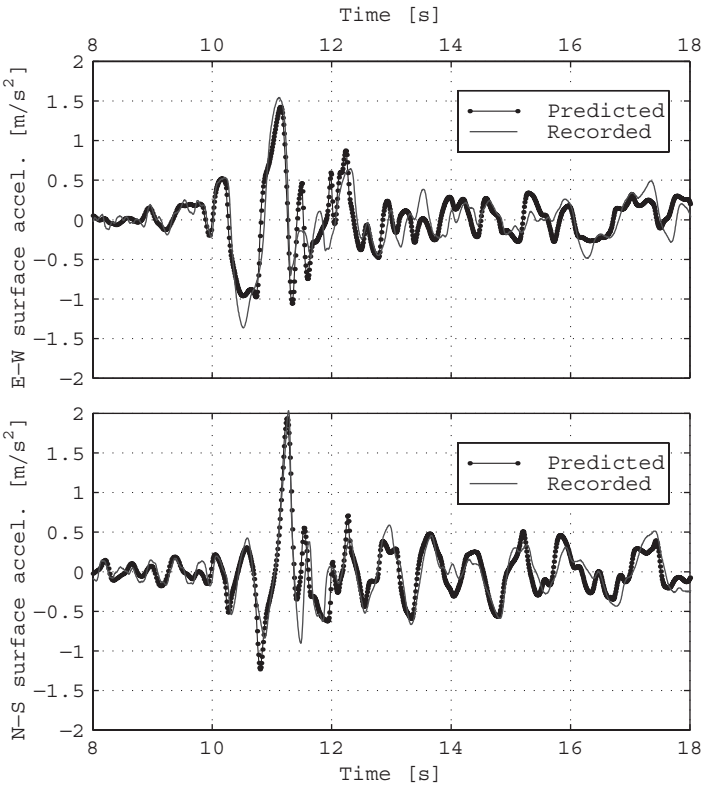

Figure 8. Simulation of the surface free-field response during the LSST07 seismic event in Lotung, Taiwan: (a) E–W acceleration; and (b) N–S acceleration.

herein show similar coupling behaviour. The data of those stress-point examples correspond basically to those obtained for the soil at 35–47 m depth. The time-integration procedure is the generalized mid-point algorithm of Simó *et al.* [29]. The parameters of the model are summarized in Table II.

10. DISCUSSION

In comparison to other models with similar characteristics, the model presented in this work as well as the model of Reference [8] are derived from the principle of maximum dissipation which gives them a sound mathematical foundation. If we assume that the hardening function derives from a potential and that the principle of maximum dissipation is to be preserved, Equations (14) and (16) suggest Prager's rule. This is not an impediment for the development of multilayer and bounding surface plasticity fulfilling those assumptions. For the first type of models, Reference [8] is an example. For the second type of models, the present work shows that. In addition, both models present a series of attractive features both from the theoretical and the numerical point of view. First, they do not use *ad hoc* geometrical translation rules for

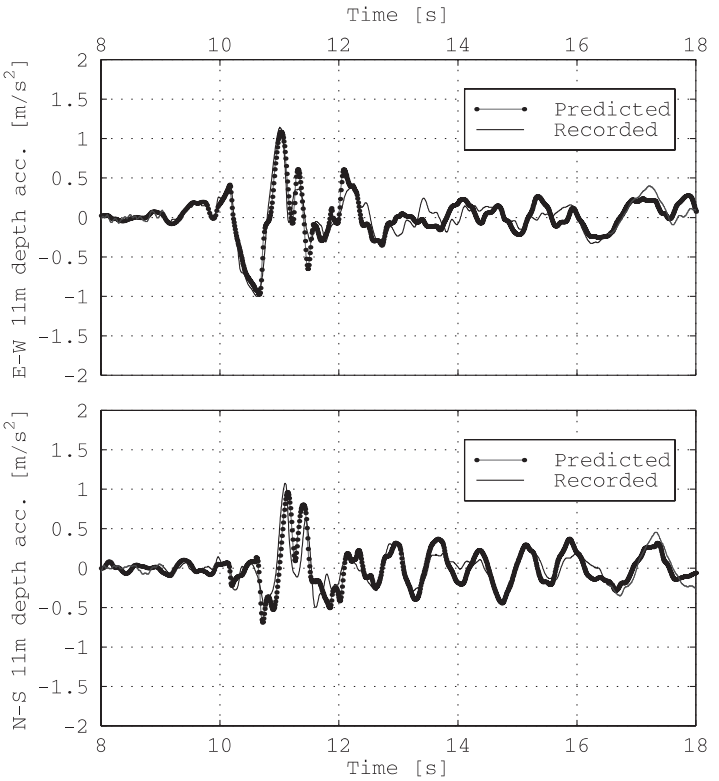

Figure 9. Simulation of the free-field response at 11 m depth during the LSST07 seismic event in Lotung, Taiwan: (a) E–W acceleration; and (b) N–S acceleration.

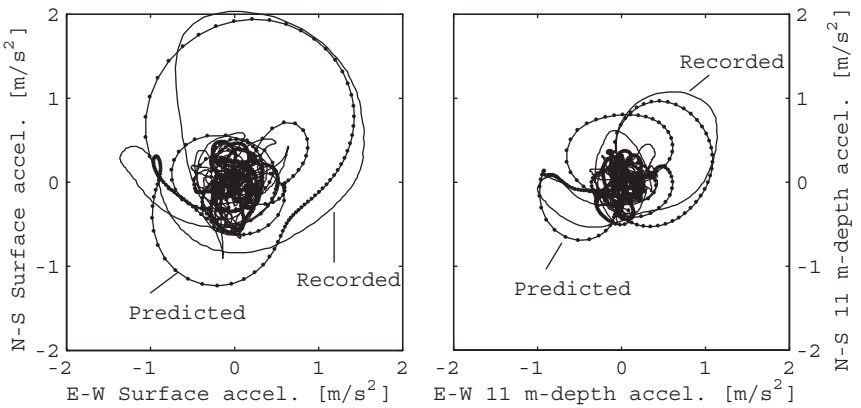

Figure 10. Coupling of the free-field response during the LSST07 seismic event in Lotung, Taiwan: (a) Surface acceleration; and (b) 11 m depth acceleration.

Table II. Data for the Lotung analysis.

Number of elements for vertical-propagating waves: 47 of 1 m depth each
Shear moduli profile: from 25 to 180 MPa see Reference [21]
Poisson's ratio $\nu = 0.48$ and density $\rho = 19.0\,\mathrm{kN/m^3}$ for the whole soil column
Prescribed points of the shear moduli degradation curve for the whole soil column, see Reference [25]:
$\{(\mu/\mu_{\max} = 0.81, \gamma = 0.01\%), (0.375, 0.1\%), (0.1, 1\%)\}$ (from resonant column experiments)
Mid-point time integration parameters: $\theta = 0.95$, Newmark $\beta = 0.276$ and Newmark $\gamma = 0.55$
Input motion: simultaneously N–S and E–W components recorded at 47 m depth
Time increment: $\Delta t = 0.08$ s until $t = 8$ s, $\Delta t = 0.01$ s thereafter, resulting in a total of 1100 steps
Number of allowable surfaces: 5 (includes yield and bounding surfaces)
Number of Simpson intervals $2n = 2$
Viscous damping: 0.5% of the elastic, maximum stiffness (from experimental curves)
Relative euclidean tolerance over the norm of residual forces: 1.0×10^{-5}
Maximum number of iterations per step: 6; mean number of iterations per step: 3.2
Elapsed time (in a Pentium III 733 MHz): 2 min 52 s

the yield surface (i.e. Mróz's rule), but only for the hardening surfaces. Second, they do not use concepts like 'loading surface', since consistency is always applied at the yield surface. Third, in contrast to models based on the Mróz rule, the Prager translation rule of the yield surface is consistent, it does not depend on the number or dimensions of the surfaces since for bilinear behaviour classical J_2-plasticity is recovered (see Reference [31]). They yield radial return implicit numerical algorithms, which are robust, unconditionally convergent and consistently linearized in order to obtain asymptotic second-order convergence when using Newton algorithms. In contrast with other algorithms presented in References [9, 17] for models using Mróz's rule, these models do not require complex step partitionings nor any relative size between adjacent surfaces.

Aside, the model herein presented preserves Masing's rules as multilayer plasticity does, but it has its own features. In monotonic or proportional cyclic plasticity of increasing amplitude the yield and bounding surfaces are sufficient for an accurate representation (in contrast with multilayer plasticity), whereas in the rest of the cases a small amount of surfaces (3–4) will suffice to attain good results, independently of the magnitude of the stresses (the size of the surfaces will always be automatically optimal). The user does not have to worry about obtaining a good ratio and amount of surfaces for his/her own specific problem and the needed amount of memory is significantly smaller than that of equivalent multilayer plasticity.

From the behavioural point of view, nonproportional paths mark the difference between the models using Prager's rule and Mróz's rule. It is virtually impossible to say anything conclusive about the general suitability of any rule. Nonetheless, note that in the multiaxial predictions for the Lotung problem, those with closer relation between stresses increments and strains increments were the ones that gave good results in predicting the coupling, as shown in this work and in Reference [8]. This is in agreement with the usual assumption for the behaviour of soils [20] and this idea is behind the vanishing surface concept (see Reference [30] also for a criticism applied to other models with that feature). Aside, the amount of 'hypoplastic' behaviour may be controlled in a simple way by an explicit parameter τ.

Finally, the computational cost of this model is obviously higher than that of classical bilinear plasticity and, frequently, than that of multilayer plasticity. But whereas the computational

effort in the material routine is of the order of the number of integration points, the computational cost of solving the system of equations is usually of the order of n^2 or n^3 (depending on the algorithm, being n the number of degrees of freedom) which dominates over the former for large problems.

11. CONCLUSIONS

A bounding surface model for J_2-plasticity is presented. The model has similar features to many classical anisotropic J_2-models; in fact, it may be argued that the present model is the classical plasticity model of Reference [24] but with a different way of prescribing the hardening function. This feature is similar to that of the multilayer model using Prager's translation rule presented earlier. However, the present model shows a way to reformulate bounding surface plasticity conforming with the principle of maximum plastic dissipation without sacrificing some desired features such as nonlinear hardening functions and unloading-event location without added inaccuracies.

The model has been implemented using an implicit algorithm amenable to consistent linearization, preserving the asymptotic quadratic convergence rate of the Newton iterations. Stress-point-level examples showed that, for a prescribed stress, the strain path predicted by the present model qualitatively lies between that of multilayer plasticity using Mróz's rule and that using Prager's rule; but this feature may be easily modified *a posteriori* without altering the convergence and stability properties of the implicit algorithm. The resulting model may behave in a 'hypoplastically' controlled way with vanishing elastic region. This feature is attained using an associative formulation both in flow and hardening rules and is desirable for many materials, specially for soils. The model has been applied to the prediction of the free-field response of the well-known LSST07 seismic event in Lotung, Taiwan.

ACKNOWLEDGEMENTS

The authors would like to thank the anonymous reviewers of Reference [8] whose comments motivated in part the present work. The second author acknowledges the support of the US National Science Foundation under Contract No. CMS-9613906 through the direction of Dr. C. S. Astill. The digitalized data for the Lotung data were provided by Dr H. T. Tang of the Electric Power Research Institute. All of these supports are gratefully acknowledged.

REFERENCES

1. Simó JC, Hughes TJR. *Computational Inelasticity*. Springer: New York, 1998.
2. Lemaitre J, Chaboche J-L. *Mechanics of Solid Materials*. Cambridge University Press: Cambridge, 1990.
3. Kramer SL. *Geotechnical Earthquake Engineering*. Prentice-Hall: Englewood Cliffs, NJ, 1996.
4. Ishihara K. *Soil Behavior in Earthquake Geotechnics*. Clarendon Press: Oxford, 1996.
5. Mróz Z. On the description of anisotropic work-hardening. *Journal of Mechanics and Physics of Solids* 1967; **15**:163–175.
6. Iwan WD. On a class of models for the yielding behaviour of continuous and composite systems. *Journal of Applied Mechanics*, (ASME) 1967; **35**:612–617.
7. Prevost JH. Nonlinear dynamic response analysis of soil and soil–structure interacting systems—Section 4: plasticity model for frictional soils. In *Soil Dynamics and Geotechnical Earthquake Engineering*, Sêco e Pinto (ed.). Balkema: Rotterdam, 1993; 88–101.
8. Montáns FJ. Implicit multilayer J_2-plasticity using Prager's translation rule. *International Journal for Numerical Methods in Engineering* 2001; **50**:347–376.

9. Montáns FJ. Implicit algorithms for multilayer J_2-plasticity. *Computer Methods in Applied Mechanics and Engineering* 2000; **189**:673–700.
10. Dafalias YF, Popov EP. A model of nonlinearly hardening materials for complex loading. *Acta Mechanica* 1975; **21**:173–192.
11. Krieg RD. A practical two-surface plasticity theory. *Journal of Applied Mechanics* (ASME) 1975; **42**: 641–646.
12. Borja RI, Tamagnini C. Cam-Clay plasticity, part III: extension of the infinitesimal model to include finite strains. *Computer Methods in Applied Mechanics and Engineering* 1998; **155**:73–95.
13. Hermann LR, Kaliakin V, Shen CK, Mish KD, Zhu ZY. Numerical implementation of plasticity model for cohesive soils. *Journal of Engineering Mechanics* (ASCE) 1987; **113**:500–519.
14. Borja RI, Amies AP. Multiaxial cyclic plasticity model for clays. *Journal of Geotechnical Engineering* (ASCE) 1994; **120**: 1051–1070.
15. Manzari MT, Nour MA. On implicit integration of bounding surface plasticity models. *Computers and Structures* 1997; **63**:385–395.
16. Borja RI, Lin C-H, Montáns FJ. Cam-Clay plasticity, part IV: implicit integration of anisotropic bounding surface model with nonlinear hyperelasticity and ellipsoidal loading function. *Computer Methods in Applied Mechanics and Engineering* 2001; **190**:3293–3323.
17. Montáns FJ. Bounding surface plasticity model with extended Masing behaviour. *Computer Methods in Applied Mechanics and Engineering* 2000; **182**:135–162.
18. Kahn AS, Huang S. *Continuum Theory of Plasticity*. Wiley: New York, 1995.
19. Dafalias YF. Bounding surface plasticity. I: mathematical foundation and hypoplasticity. *Journal of Engineering Mechanics* (ASCE) 1986; **112**:966–987.
20. Dafalias YF. Overview of constitutive models used in VELACS. In *Verifications of Numerical Procedures for the Analysis of Soil Liquefaction Problems*, Alurandan K and Scott RF (eds). Balkema: Rotterdam, 1994; 1293–1303.
21. Borja RI, Chao HY, Montáns FJ, Lin CH. Nonlinear ground response at Lotung LSST site. *Journal of Geotechnical and Geoenvironmental Engineering* (ASCE) 1999; **125**:187–197.
22. Borja RI, Chao HY, Montáns FJ, Lin CH. SSI effects on ground motion at Lotung LSST site. *Journal of Geotechnical and Geoenvironmental Engineering* (ASCE) 1999; **125**:760–770.
23. Hildebrand, FB. *Introduction to Numerical Analysis*. Dover: New York, 1987.
24. Simo JC, Taylor RL. Consistent tangent operators for rate-independent elasto-plasticity. *Computer Methods in Applied Mechanics and Engineering* 1985; **48**:101–118.
25. EPRI, Gidelines for determining design basis ground motions, vol 1: method and guidelines for estimating earthquake ground motion in Eastern North America. *Technical Report No. TR*-102293, Electric Power Research Institute (EPRI), Palo Alto, 1993.
26. Anderson DG. Geotechnical sintesis for the Lotung large-scale seismic experiment. *Technical Report No. TR*-102362, Electric Power Research Institute (EPRI), Palo Alto, 1993.
27. Elgamal A-W, Zeghal M, Tang HT, Stepp JC. Lotung downhole array I: Evaluation of site dynamic properties, and II: Evaluation of soil nonlinear properties. *Journal of Geotechnical Engineering* (ASCE) 1995; **121**: 350–377.
28. Montáns FJ, Borja, RI. Modelo de plasticidad multiaxial para arcillas sometidas a carga dinámica. *Revista Internacional de Métodos Numéricos para Cálculo y Diseño en Ingeniería* 1999; **15**:169–192.
29. Simó JC, Tarnow N, Wong K. Exact energy-momentum conserving algorithms and symplectic schemes for nonlinear dynamics. *Computer Methods in Applied Mechanics and Engineering* 1992; **100**:63–116.
30. Hashiguchi K. A mathematical modification of two surface model formulation in plasticity. *International Journal of Solids and Structures* 1988; **24**:987–1001.
31. Jiang Y, Sehitoglu H. Comments on the Mróz multiple surface type plasticity models. *International Journal of Solids and Structures* 1996; **33**:1052–1068.

